OAK RIDGE
NATIONAL LABORATORY
MANAGED BY UT-BATTELLE
FOR THE DEPARTMENT OF ENERGY

ORNL/TM-2009/313

Design Study for a Low-Enriched Uranium Core for the High Flux Isotope Reactor, Annual Report for FY 2009

February 2010

Prepared by
R. T. Primm III
D. Chandler
J. D. Freels
T. Guida
G. Ilas
B. C. Jolly
J. H. Miller
J. D. Sease

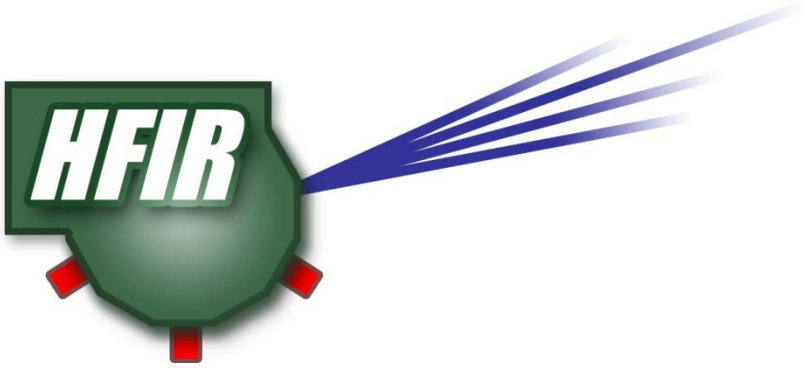

UT-BATTELLE
ORNL-27 (4-00)

ORNL/TM-2009/313

DESIGN STUDY FOR A LOW-ENRICHED URANIUM CORE FOR THE HIGH FLUX ISOTOPE REACTOR, ANNUAL REPORT FOR FY 2009

R. T. Primm III
D. Chandler
J. D. Freels
T. Guida*
G. Ilas
B. C. Jolly
J. H. Miller
J. D. Sease

*University of Pittsburgh

Date Published: February 2010

Prepared by
OAK RIDGE NATIONAL LABORATORY
Oak Ridge, Tennessee 37831-6283
managed by
UT-BATTELLE, LLC
for the
U.S. DEPARTMENT OF ENERGY
under contract DE-AC05-00OR22725

CONTENTS

Page

LIST OF FIGURES

Figure **Page**

LIST OF TABLES

ACKNOWLEDGMENTS

The authors would like to acknowledge that the support for this project was provided by the Global Threat Reduction Initiative, Reduced Enrichment for Research and Test Reactors Program (RERTR), Nuclear National Security Administration, U.S. Department of Energy (DOE). The DOE program manager, Parrish Staples, Idaho National Laboratory RERTR program manager, Dana Hewitt, and Argonne National Laboratory RERTR reactor analysis program manager, John Stevens, all provided useful comments and reviews of this work during the fiscal year. The authors also acknowledge the technical reviews of this document performed by D. G. Renfro and K. A. Smith, both of Research Reactors Division, Oak Ridge National Laboratory, and thank all of the reviewers for their efforts and comments. Finally, the authors wish to thank Mary Wells for document preparation and editing of this report.

FOREWORD

The format of this annual report is changed from that of previous years. The goal of this and future annual reports will be briefly describe accomplishments and refer the reader to topical reports on the subject matter. Detailed technical descriptions will, in general, not be included in the report. In those instances where the content of a study was insufficient to merit a separate topical report, the study will be presented in an appendix to this report with minimal discussion in the body of the report.

OTHER REPORTS IN THIS SERIES

R. T. Primm III, R. J. Ellis, J. C. Gehin, D. L. Moses, J. L. Binder, and N. Xoubi, *Assumptions and Criteria for Performing a Feasibility Study of the Conversion of the High Flux Isotope Reactor Core to Use Low-Enriched Uranium Fuel*, ORNL/TM-2005/269, February 2006.

R. T. Primm III, R. J. Ellis, J. C. Gehin, K. T. Clarno, K. A. Williams, and D. L. Moses, *Design Study for a Low-Enriched Uranium Core for the High Flux Isotope Reactor, Annual Report for FY 2006*, ORNL/TM-2006/136, November 2006.

J. D. Sease, R. T. Primm III, and J. H. Miller, *Conceptual Process for the Manufacture of Low-enriched Uranium/Molybdenum Fuel for the High Flux Isotope Reactor*, ORNL/TM-2007/39, September 2007.

R. T. Primm III, R. J. Ellis, J. C. Gehin, G. Ilas, J. H. Miller, and J. D. Sease, *Design Study for a Low-Enriched Uranium Core for the High Flux Isotope Reactor, Annual Report for FY 2007*, ORNL/TM-2007/45, November 2007.

D. Chandler, R. T. Primm, III, and G. I. Maldonado, *Validating MCNP for LEU Fuel Design via Power Distribution Comparisons*, ORNL/TM-2008/126, November 2008.

Lee Tschaepe, Arthur E. Ruggles, James D. Freels, and R. T. Primm, III, *Evaluation of HFIR LEU Fuel Using the COMSOL Multiphysics Platform*, ORNL/TM-2008/188, March 2009.

C. Galvez Velit, R. T. Primm III, and J. C. Gehin, *Partial Safety Analysis for a Reduced Uranium Enrichment Core for the High Flux Isotope Reactor*, ORNL/TM-2007/226, April 2009.

R. T. Primm III, D. Chandler, G. Ilas, B. C. Jolly, J. H. Miller, and J. D. Sease, *Design Study for a Low-Enriched Uranium Core for the High Flux Isotope Reactor, Annual Report for FY 2008*, ORNL/TM-2009/87, March 2009.

D. Chandler, R. T. Primm, III, and G. I. Maldonado, *Validation of a Monte Carlo Based Depletion Methodology with HFIR Post-Irradiation Examination Data*, ORNL/TM-2009/123, July 2009.

G. Ilas and R. T. Primm, III, *Fuel Grading Study on a Low-Enriched Uranium Fuel Design for the High Flux Isotope Reactor*, ORNL/TM-2009/223, November 2009.

Tracey Guida and R. T. Primm, III, *Establishing a Cost Basis for Converting the High Flux Isotope Reactor from High Enriched to Low Enriched Uranium Fuel*, ORNL/TM-2009/311, February 2010.

ABSTRACT

This report documents progress made during FY 2009 in studies of converting the High Flux Isotope Reactor (HFIR) from high enriched uranium (HEU) fuel to low enriched uranium (LEU) fuel. Conversion from HEU to LEU will require a change in fuel form from uranium oxide to a uranium-molybdenum alloy. With axial and radial grading of the fuel foil and an increase in reactor power to 100 MW, calculations indicate that the HFIR can be operated with LEU fuel with no degradation in reactor performance from the current level. Results of selected benchmark studies imply that calculations of LEU performance are accurate. Studies are reported of the application of a silicon coating to surrogates for spheres of uranium-molybdenum alloy. A discussion of difficulties with preparing a fuel specification for the uranium-molybdenum alloy is provided. A description of the progress in developing a finite element thermal hydraulics model of the LEU core is provided.

1. INTRODUCTION

Design studies for a low-enriched uranium (LEU) core for the High Flux Isotope Reactor (HFIR) were conducted according to the plan documented in ref. 1. Lists of the studies that had been planned for fiscal year (FY) 2009 — published in ref. 1 — are shown in Tables 1.1 and 1.2. Progress in reactor analysis studies and material development are presented in separate sections of this report. The final section of this report is devoted to a discussion of tasks planned for FY 2010.

Table 1.1. Reactor analysis activities proposed for FY 2009

Task area	Subtask	
	Title	Description
Reference U-10Mo fuel design (axial grading of foil)	Neutronics/thermal hydraulics design	Document neutronics and thermal hydraulics studies of reference LEU-10Mo design
	Process development	Develop and document engineering drawings and fuel specification for reference LEU fuel
	Computation model verification/validation	Compare ALEPH/MCNP to post-irradiation HEU measurements
Transition cycles (modify current HEU fuel to achieve LEU design burnup)	Neutronics	Determine U-235 loading and grading profile
	Process development	Determine changes to existing process to create higher-loaded HEU fuel plates
Improved U-10Mo fuel design (no axial grading)	Development of COMSOL based methodology	Multidimensional, steady state heat transfer model; turbulent mixing, incorporate diffusion barrier and nonbond assumptions in thermal-hydraulic model
	Thermal hydraulic committee	---
Preparation for regulatory review	Research publications for LEU validation; develop plan for LEU validation studies	---
Methods/model development	Cross section processing	Document 2-D SCALE model
	Deterministic methods implementation	Transport methods (ATTILA model); REBUS model
	Upgrade Monte Carlo Depletion methods	Migrate from ALEPH software to VESTA software
	Probabilistic combination of uncertainties (if funding is available)	Review/update TASHA code developed under Advanced Neutron Source Program
Program management	---	Report preparation
		Travel
		Meeting attendance

Table 1.2. ORNL fuel development activities proposed for FY 2009

Task name	Comment
Graded fuel development program	Perform tasks as identified by Idaho National Laboratory
Fuels program management	Includes support to review committees, meeting attendance, travel, and report preparation

2. REACTOR ANALYSES

The goal of reactor analyses in FY 2009 was to confirm that High Flux Isotope Reactor (HFIR) performance with a reactor fuel based on low enriched (19.75 wt %) uranium-molybdenum alloy (90 wt % uranium, 10 wt% molybdenum; termed U-10Mo) could be maintained at the same level as with the current, high enriched (HEU) fuel. This goal was accomplished as documented in the September 29, 2009 letter from K. J. Beierschmitt, Oak Ridge National Laboratory (ORNL) to Parrish Staples, National Nuclear Security Administration (NNSA).

Verified and validated neutronics methods were used to develop a reference U-10Mo design. Studies of an advanced, simplified U-10Mo fuel plate continued with three dimensional, finite-element based methods with the goal of replacing the capabilities available from an existing, one dimensional conduction computer program[2]. Other activities included consideration of fuel qualification issues and further refinement of a schedule for conversion of the HFIR to LEU fuel.

2.1 Reference U-10Mo Fuel Design

Currently used neutronics methods for the design of an LEU core are considerably advanced beyond the level of technology used in the design of the HFIR HEU fuel. Thermo-hydraulic-mechanical behavior of the LEU core is still analyzed with methods developed for the HEU fuel in the late 1960s.[2] With these tools, engineering analyses indicate that LEU fuel will have to be graded (spatial variation in fuel thickness) in both the radial and axial direction whereas the current HEU fuel is only graded radially. With two dimensional grading and an increase in reactor power to 100 MW from the current value of 85 MW, the flux performance at selected experimental locations (both magnitude of the flux and energy spectral distribution) is essentially unchanged from current operation.

2.1.1 Neutronics/thermal hydraulics design

Physics methods, fuel grading studies, and reactor performance are documented in ref. 3. Only the lowermost 3 cm of the fuel foil will be graded axially and radially. The remainder of the foil (47.8 cm length) will be graded radially. Further refinement of the radial and axial grading profiles requires definition of and input from the fuel fabrication processes.

2.1.2 Fuel specification (fabrication process development)

Though LEU fuel fabrication is not the responsibility of ORNL, the LEU fuel specification for HFIR will be the responsibility of the contracting operator for HFIR. During this year, considerable thought was given to developing a HFIR fuel element specification for an LEU foil fuel. Using the current HFIR fuel element specification for the HEU dispersion fuel,[4] an attempt was made to modify this document for the LEU foil fuel. Drafts of several sections from this specification were attempted but it was apparent that the fabrication data to support this type of specification do not exist.

Modifications to the detailed flow sheets presented in ref. 5 were attempted to identify the inspection points required to develop a specification for a LEU foil fuel. It was apparent that information on the foil properties (i.e., uranium composition, trace elements, alloy homogeneity, grain size and mechanical properties) required for developing and controlling the contour forming process had not been generated. In flat foil development, very limited data are available on allowed tolerance variations in the thickness of the foils (i.e., statistical process capabilities data) and the thickness and allowed tolerance variations in the co-rolled zirconium diffusion barrier.

Available specifications for the requirements of the zirconium diffusion barrier bonding to the U/Mo foil and the aluminum cladding are very limited to nonexistent. No information is available on the allowed defect level, inspection method, and inspection standards. Data for the forming of the foils into the involute shape required in the assembly of the HFIR fuel elements and the defects induced into plates from forming do not exist. Methods for inspecting for possible defects in formed plates do not exist. Also the impact of formed HFIR LEU fuel plates on channel spacing is unknown (differences from the behavior of current, HEU fuelled plates).

At this point it is apparent that an updated, detailed reference flow sheet similar to the ones shown in ref.5 is urgently needed. These flow sheets should tentatively identify all inspection points and requirements that will be needed to develop a fuel element specification. In any manufacturing process, the principal axiom to total quality management is "if you cannot measure the process parameters you cannot control the process."

2.1.3 Computational model verification/validation

The only reactors known to have operated or proposed to have been operated with uranium-molybdenum metal fuel (the Health Physics Research Reactor and the organic cooled and moderated reactor) are not typical of HFIR geometry, configuration, or neutron energy spectra. Consequently the best method for validating HFIR neutronics methods is to use critical experiment data and reactor operating data for the current, HEU fuel. Results of the ability to accurately calculate reactor cycle length by modeling a current fuel cycle[1] and the ability to predict power distribution within the reactor by modeling critical experiments[6] were reported last fiscal year. This fiscal year, studies were conducted to compare end-of-cycle measured uranium isotopic spatial distributions with calculated values.[7] Agreement was very good and indicated, in an integral sense, good ability of the neutronics methods to calculate spatial power distributions at all irradiation times during the fuel cycle.

No further validation studies are planned for the near term though some existing, non-HFIR-geometry LEU critical experiments could be useful for validating future criticality safety analyses for fuel storage and transportation. Conversion of the other, U.S. high performance reactors to LEU fuel may be another source of useful validation measurements.

2.2 Transition Cycles

A transition cycle, for HFIR, was proposed as modifying the current HEU fuel to achieve the design basis, end-of-cycle burnup expected for LEU fuel. (Since the LEU fuel cycle operates at a higher power level than the current HEU cycle — 100 MW vis-à-vis 85 MW — maintaining the same cycle length in days yields an LEU end-of-life burnup greater than that of the current, HEU fuel cycle.) Upon review of the proposal, the program office directed that, "the HEU parity issue is not considered HEU minimization, nor do we want to support that from the NNSA perspective" and "this demonstration is not in line with GTRI's mission goals and presentation of the novel approach could jeopardize international partnerships on reactor conversions." Consequently these studies were terminated.

2.3 Improved U-10Mo Fuel Design

Removal of the axial grading requirement for LEU fuel would simplify the fuel fabrication process. This design requirement is believed to result from unnecessarily conservative approximations in the current HFIR thermo-hydraulic-mechanical analysis program.[2] State-of-the-art three dimensional, finite element based methods will remove some of the unnecessary conservatism due to current methods being limited to one-dimensional heat transport.

2.3.1 Development of COMSOL based methodology

The finite element methodology was instigated in FY 2008 and the results of initial studies are documented in ref. 8. Various problems encountered in FY 2008 related to mesh generation, boundary layer treatments, and comparison to the current HFIR analysis methodology were resolved during FY 2009 and some of this work is documented in ref. 9. Since conference proceedings are not always readily available, ref. 9 is reprinted in this document as Appendix A.

2.3.2 Thermal hydraulic committee

The committee was formed and met for the first time at Argonne National Laboratory on Feb. 3-4, 2009. An analytic benchmark problem, proposed by University of Missouri, provides an initial area of mutual computational investigation. The development of a flow test loop at Oregon State University provides for mutual development of experiments.

2.4 Other Studies

The recently available depletion simulation tool, VESTA, was received at ORNL. The computational package has the same author as ALEPH and is based on the same methodology but with extended computational capabilities. This Monte Carlo depletion capability will be implemented during FY 2010 and verified and validated with previously constructed HFIR ALEPH models.

2.4.1 Cost/schedule for HFIR conversion

A first attempt at a plan for conversion of the HFIR from HEU to LEU fuel, including tasks, costs, and schedules, was developed to provide input to the multi-reactor conversion program integrated plan. The model is documented in ref. 10. Using Microsoft Project, a detailed outline of the conversion program was established and consists of LEU fuel design activities, a fresh fuel shipping cask, improvements to the HFIR reactor building, and spent fuel operations. Current-value costs total $76 million dollars, include over 100 subtasks, and will take over 10 years to complete. The model and schedule follow the path of the fuel from receipt from fuel fabricator to delivery to spent fuel storage and illustrates the duration, start, and completion dates of each subtask to be completed. This plan is subject to revision based on feedback from the multi-reactor conversion program manager and other emerging developments.

2.4.2 Statistical assessment of the quantity of irradiation tests planned for certification of LEU fuel for HFIR

Reference 11 notes that "The AFIP-9 experiment will be focused on testing fuel plates with both burnable poison and a graded fuel zone in a full-size scale. The experiment will consist of at least two plates." The AFIP-9 experiment is currently the only irradiation experiment planned for full-size HFIR plates. Since HFIR contains two types of fuel plates — an inner element plate and an outer element plate — prudent planning for HFIR fuel qualification should be based on the irradiation of a single inner element plate and a single outer element plate although the phrase "at least" in Ref. 11 implies that the number could be larger.

Appendix B contains documentation of a statistical study conducted under the assumption that the process variables to be monitored for an LEU plate have the same manufacturing tolerances as exist for the current HEU fuel — tolerances being identified, design basis deviations from the nominal values of measured parameters. A study was conducted to determine the needed standard deviations of the measurement techniques for these parameters under the assumption that only a single fuel plate will be tested — the AFIP-9 experiment — and the probability of failure is less than 1 in 540, i.e., the initial LEU core loaded to HFIR will not fail.

The conclusion was that the ratio of design basis parameter tolerance-to-standard deviation of the measurement technique for that parameter should be at least five. That is, given the current level of planned fuel qualification, the uncertainty in the measurement technique for any given parameter should be 1/5 of the design basis tolerance value for that parameter. This finding relates to requirements reported earlier in Section 2.1.2. To date, no specification of process measurement techniques, much less the accuracy and precision thereof, has been reported to ORNL.

3. FUEL DEVELOPMENT

At the direction of INL, studies in FY 2009 were related to fluidized bed chemical vapor deposition of silicon onto surrogate dispersion fuel powder. In an effort to control the composition of the interface between the uranium-molybdenum (U-Mo) particles and the aluminum matrix in low enriched dispersion fuels, it is desirable to investigate the deposition of a layer of silicon onto U-Mo particles. To accomplish this, silicon deposition process development was done using stainless steel powder as a surrogate for the U-Mo. Specifically, fluidized bed chemical vapor deposition (FBCVD) methods using silane as a precursor to deposit a silicon layer onto representative stainless steel powders have been developed.

3.1 System Description

A schematic of the FBCVD system is shown in Fig. 3.1, and photographs of the system are provided in Figs. 3.2 and 3.3. The coating system developed for depositing Si onto surrogate dispersion fuel powder consists of a conical stainless steel coating chamber through which argon fluidizing gas and silane reactant gas flow. The gas flows are controlled by electronic mass flow controllers. The conical section of the coating chamber, where the powder charge is located, is positioned within the hot zone of the furnace to facilitate silane dissociation and thus silicon deposition on the surface of the powder. The furnace temperature is maintained by a furnace controller using a thermocouple that is inserted from the top of the furnace into the fluidized powder bed. The argon and silane supply lines are configured so that they can be evacuated and backfilled to remove air from the system prior to operation. There is a catch cup under the coating chamber where the coated powder is accumulated after the fluidizing gas is turned off. Although not shown in the flow diagram, there is a knockout pot in the exhaust line to catch any powder that becomes entrained in the exhaust gas stream and is carried out of the coating chamber. Also not shown in the flow diagram, there is an additional inert gas supply connected to the furnace exhaust line to provide additional diluents to the exhaust stream.

The process of conducting a coating run begins with the elimination of air from the supply system via a series of repeated evacuation and inert gas back-filling steps. After the supply lines have been sufficiently evacuated and back-filled, the argon fluidizing gas flow is established and the particle charge is loaded into the coating chamber. The coating chamber and exhaust lines are then purged with argon for several minutes while the furnace is brought up the desired coating temperature, thereby removing the air from the remainder of the system. After the furnace has reached the desired temperature and has been sufficiently purged, the silane reactant gas flow is established thus beginning the coating run. When the coating run is complete the silane gas and the furnace power are turned off. The coating system is allowed to purge with argon while the furnace cools. After the furnace is cooled, the argon fluidizing gas is turned off and the coated powder falls into the catch cup under the coating chamber.

3.2 Coating Experiments

A summary of coating experiments is provided in Table 3. 1. The table includes coating temperature, gas flows, and coating time. The initial experiments (experiments 1-4) were carried out using pure silane as the silicon source. Pure silane tended to react inside the flow meters which resulted in clogging. No silicon layers were observed in the first four coating experiments. Fig. 3.4 provides SEM images of polished cross sections of particles and a particle x-ray diffraction (XRD) pattern from coating run Si-3. The results from Si-3 are typical of the first four runs; silicon was not detectable in either the SEM or XRD results.

Starting with run number Si-5 a gas mixture of argon 5% silane was used instead of the pure silane. The flow meter plugging issue was solved, and due to the observation of un-reacted silane at the furnace exhaust, the coating temperature was raised slightly to increase the reaction rate of silane dissociation. SEM and XRD results for coating run Si-5 are shown in Fig. 3.5 and represent the first evidence of successful Si coating. The SEM image shows a distinct layer on the outside of the particle and the XRD phase identification indicated the presence of Si. Note that the XRD was conducted on intact coated particles and the composition derived from the XRD results is a result of diffraction from both the coating and the underlying powder.

Un-reacted silane was also observed at the furnace exhaust during Run 5, so for Run 6 the temperature was increased further to 580°C. Unfortunately, this caused deposition-induced clogging of the cone inlet. In order to sustain a high enough temperature to allow for complete silane reaction but maintain the cone inlet cool enough to mitigate clogging, the cone was lowered slightly in the furnace to position the inlet in a cooler portion of the furnace. Coating Runs 7 through 11 were conducted with varied gas flows and varied cone position within the furnace in an attempt to find a set of conditions that produced silicon coatings without excessive buildup in the cone inlet. The silane flow was also decreased to further slow deposition in the cone inlet.

Fig. 3.6 includes SEM and XRD results from powder coated in run Si-7. Fig. 3.7 and 3.8 show SEM images of polished cross sections from samples of particles in Runs 8 and 9, respectively. Silicon coatings were observed in all of these experiments, but unfortunately excessive amounts of the powder charge were becoming entrained in the gas flow and were carried out of the furnace and into the knockout pot in the furnace exhaust line. In order to prevent the entrainment of the powder, a 25μm screen was installed in the top of the coating chamber for run number Si-12. The screen proved advantageous, but still allowed the fines from the powder charge to pass into the exhaust. The SEM and XRD results from run 12 are provided in Fig. 3.9 for reference.

The powder entrainment problem was minimized in Runs 13 and 14 by extending the length of the coating chamber through the use of an extension fixture (see Fig. 3.3) that provided a section of increased inside diameter above the existing coating chamber. This larger section provided more length to the chamber and the increased inside diameter reduced the gas velocity. Both the increased length and the reduced gas velocity allowed the majority of the entrained powder to fall back into the fluid bed. Using the extension piece on the coating chamber reduced the losses from powder entrainment to less than 1%.

Even with the chamber extension installed, a small portion of the powder charge is still ejected from the fluid bed. Fig. 3.10 provides a photographic comparison of uncoated powder, coated powder from Si-13 (with the extension installed), and powder from the knockout pot of Si-13. The photographs show the powder that is ejected from the coating chamber consists primarily of the smaller particles from the original size distribution. Although it was not tried, it is possible that removing the fines from the powder prior to coating would help further alleviate the powder entrainment issue.

The SEM and XRD results from Runs 13 and 14 are shown in Fig. 3.11 and 3.12, respectively. The results demonstrate that reproducible deposition of a silicon layer onto surrogate fuel powder is feasible.

3.3 Conclusions

The work to date demonstrates that a silicon layer can be applied to surrogate dispersion fuel powder. The average thickness of the layer can be controlled by coating time from sub-micron to an estimated 10 microns (coating thicknesses greater than ~5 microns were not attempted but are thought feasible). The density of the stainless steel surrogate powder is less than that of the U-Mo; therefore the transition to U-Mo will require some additional process development.

Table 3. 1. Summary of Si coating experiments

Run number Si-	Coating temperature (°C)	Run time (min.)	Total gas flow (sccm)	SiH_4 (% of TGF)
1	500	Furnace malfunction		
2	500	120	1100	9.1
3	500	120	1100	9.1
4	500	160	1000	30.0
5	537	120	1000	5.0
6	580	120	1000	5.0
7	570	120	2500	1.0
8	570	120	2500	2.0
9	570	240	2000	1.3
10	570	240	2000	1.3
11	575	240	2000	1.3
12	580	180	2000	1.3
13	580	120	2000	1.3
14	580	125	2000	0.6

1. Coating batch weight for all runs 12g
2. Runs 1-3 used pure SiH_4, all subsequent runs used 5% SiH_4 in Ar.
3. TGF is total gas flow.

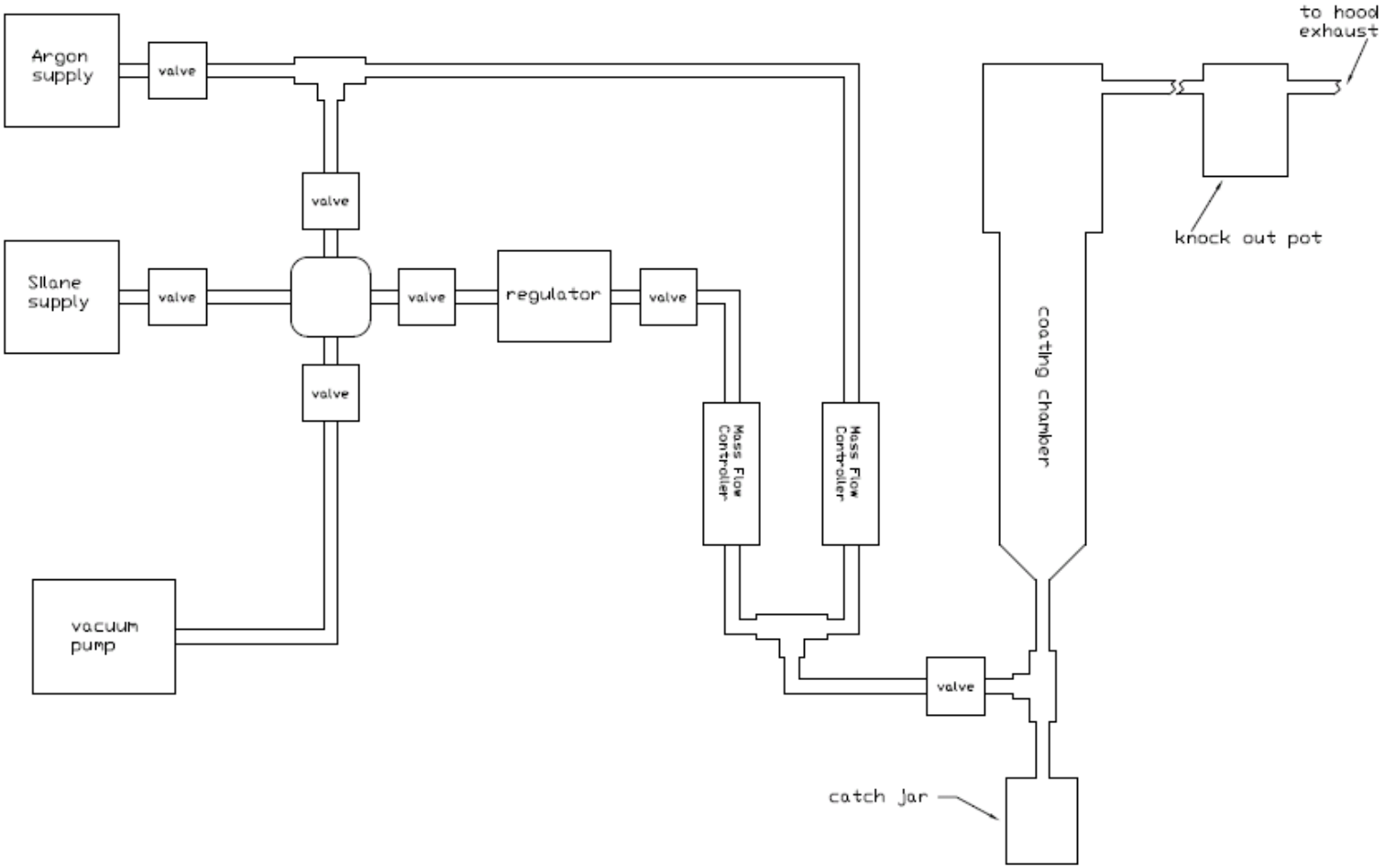

Fig. 3.1. Schematic flow diagram of the powder coating system.

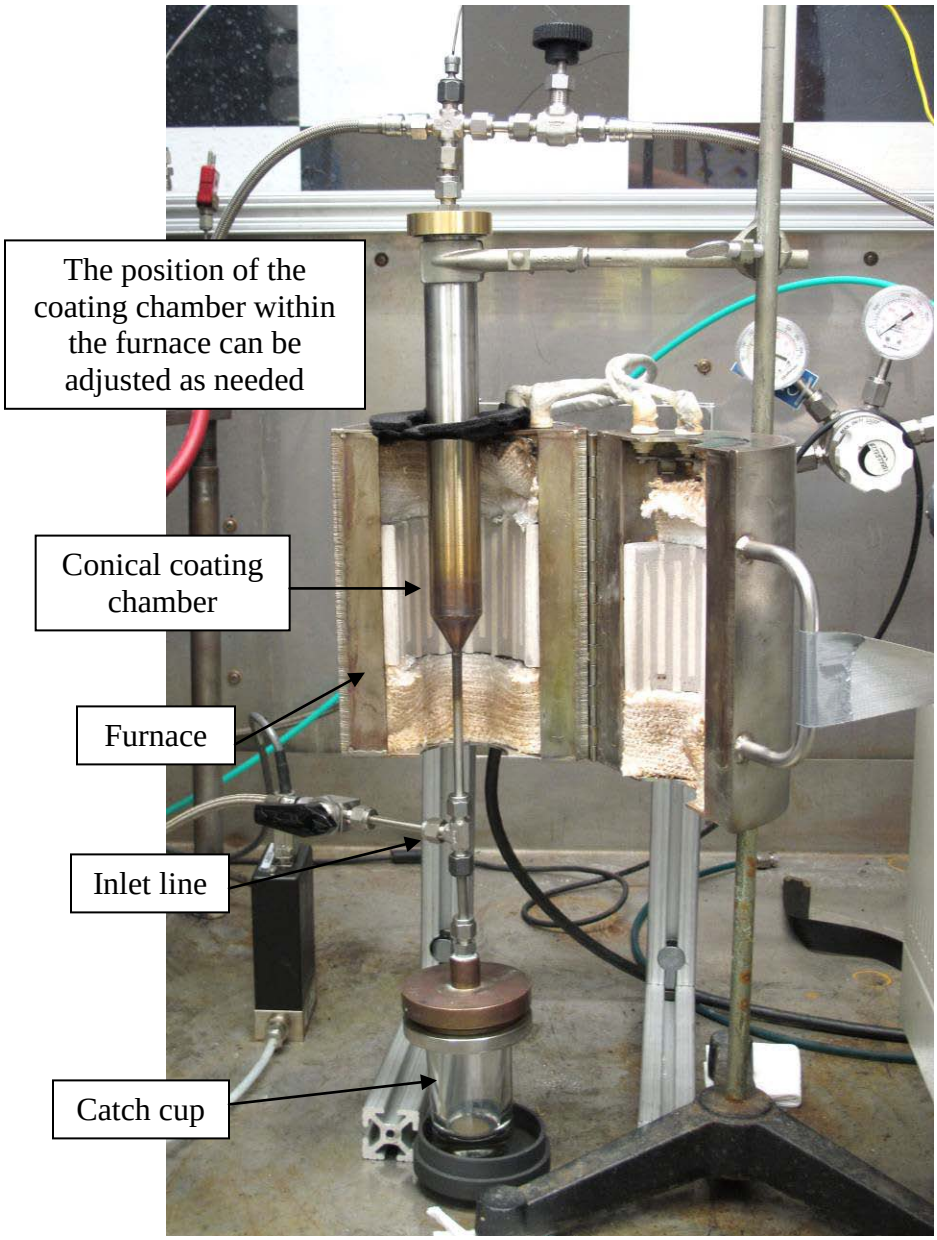

Fig. 3.2. Photograph of the powder coating furnace and chamber.

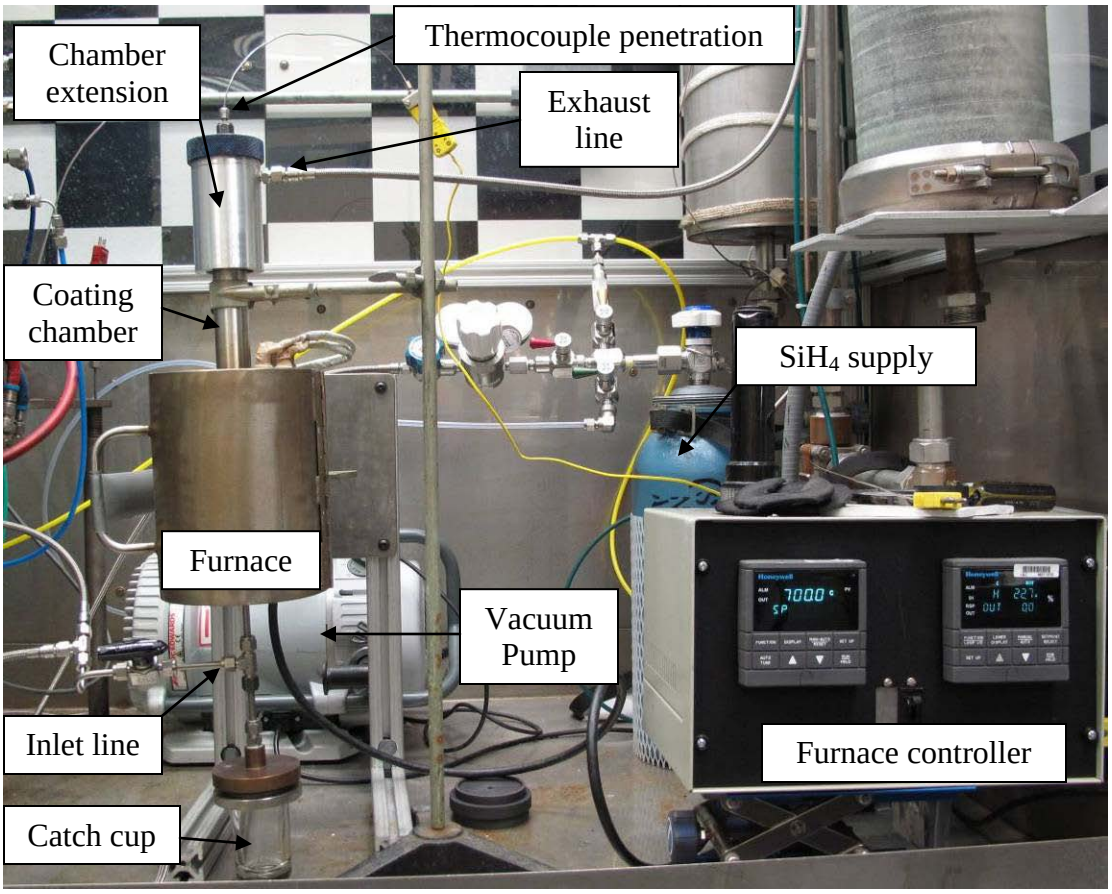

Fig. 3.3. Photograph of the powder coating system showing the chamber extension, vacuum pump and furnace controller.

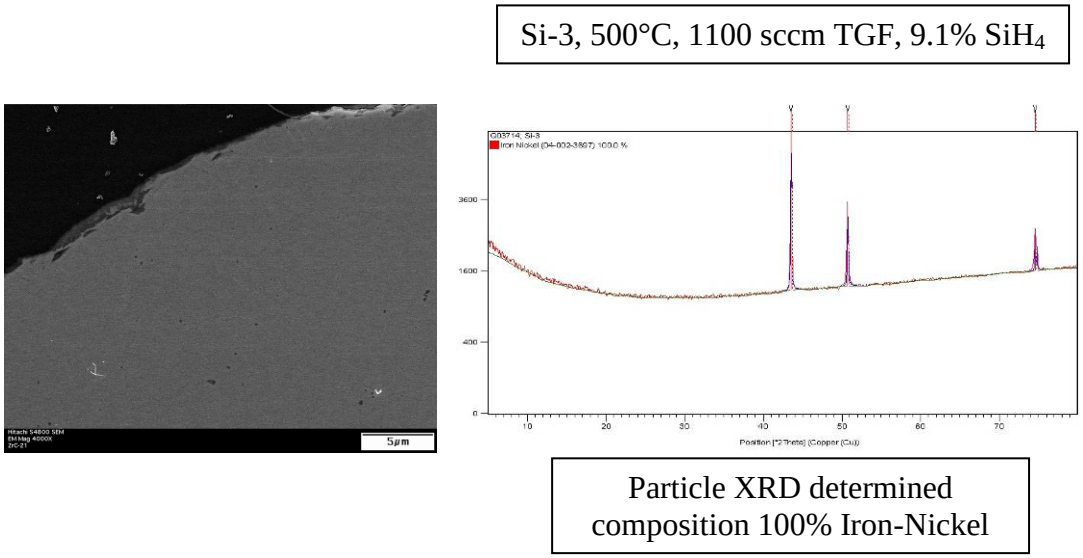

Fig. 3.4. SEM and XRD results for Si-3.

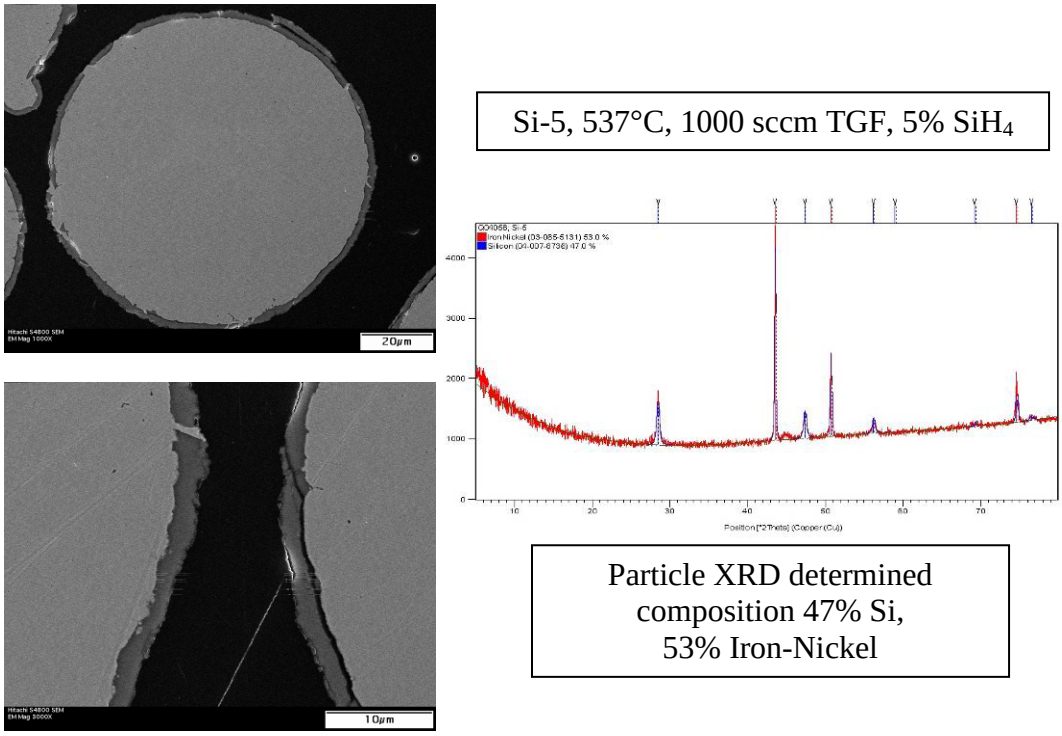

Fig. 3.5. SEM and XRD results for Si-5.

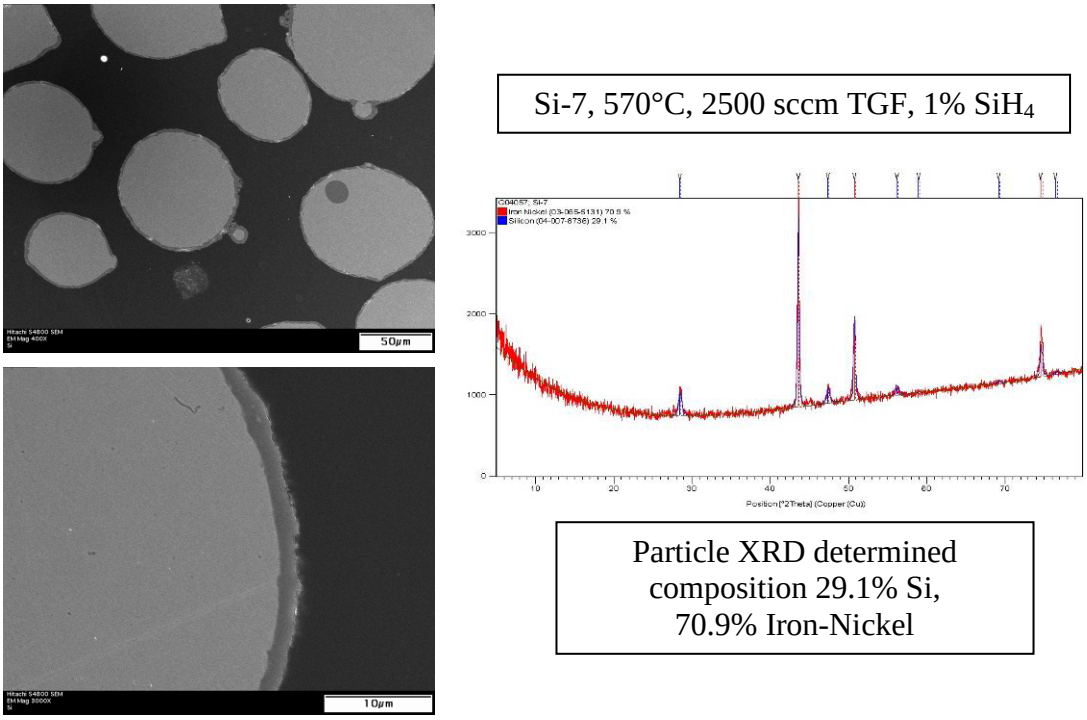

Fig. 3.6. SEM and XRD results for Si-7.

Si-8, 570°C, 2500 sccm TGF, 2% SiH_4

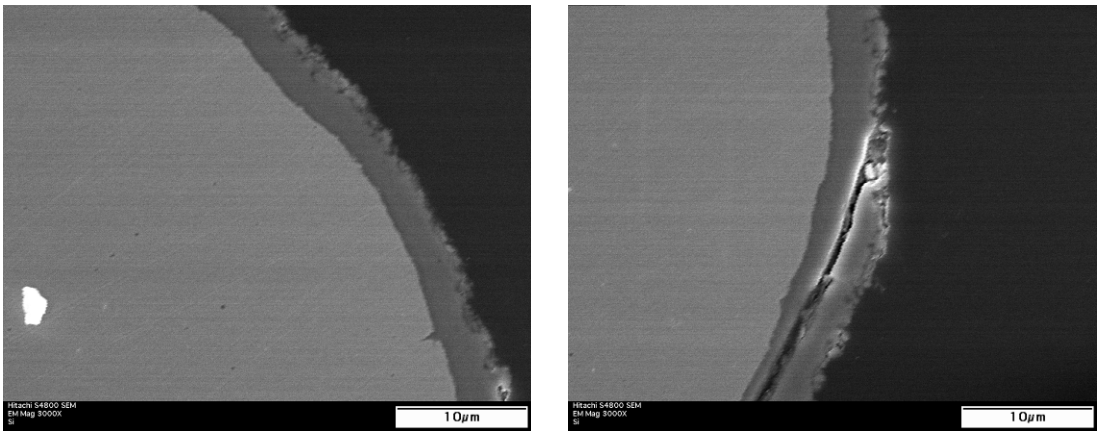

Fig. 3.7. SEM results for Si-8.

Si-9, 570°C, 2000 sccm TGF, 1.3% SiH_4

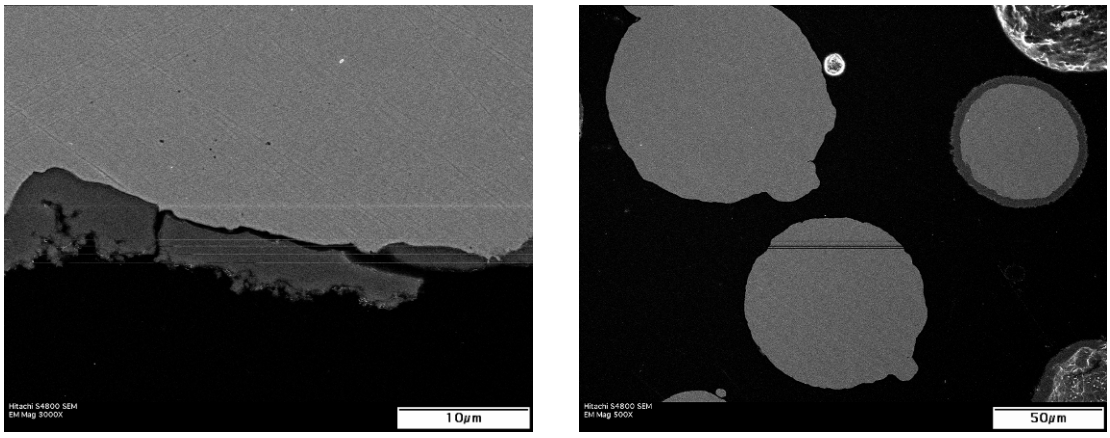

Fig. 3.8. SEM results for Si-9.

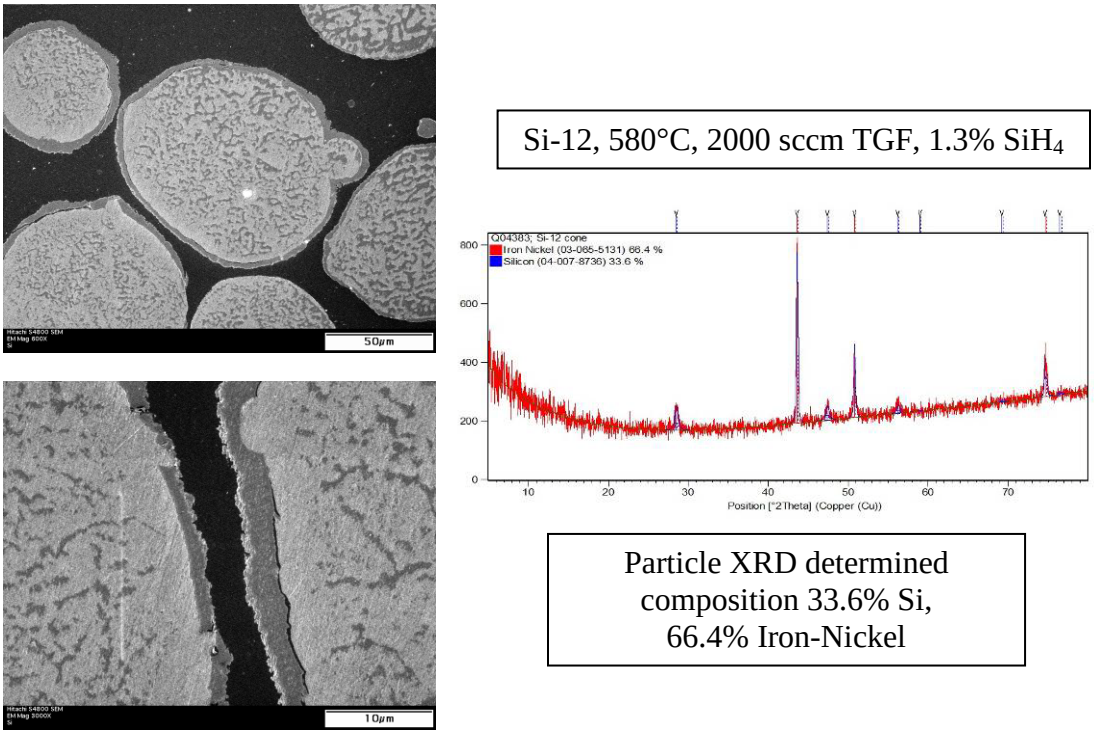

Fig. 3.9. SEM and XRD results for Si-12.

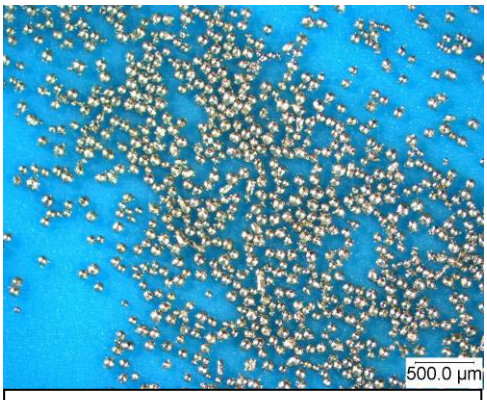

Uncoated SST powder

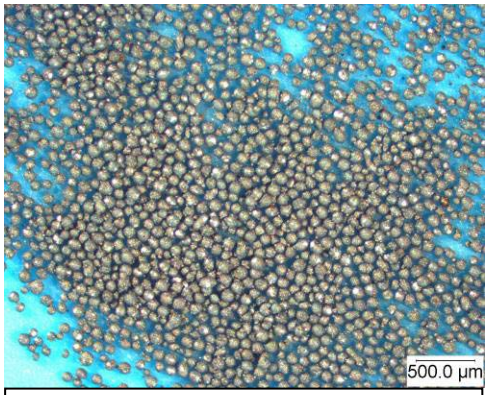

Coated powder (Si-13)

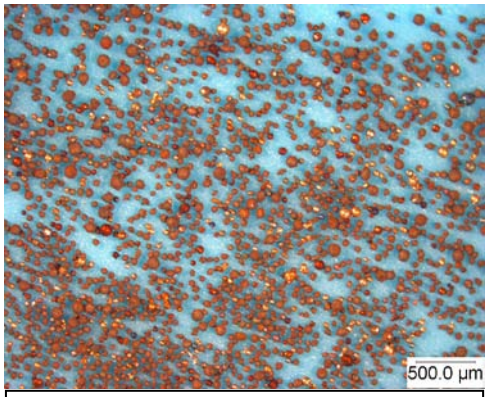

Ejected powder
(Si-13 knockout pot)

Fig. 3.10. Photographs of uncoated, coated, and ejected powders.

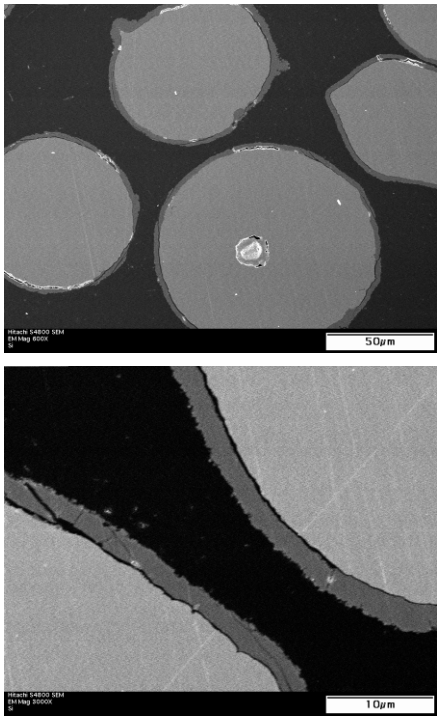

Si-13, 580°C, 2000 sccm TGF, 1.3% SiH_4

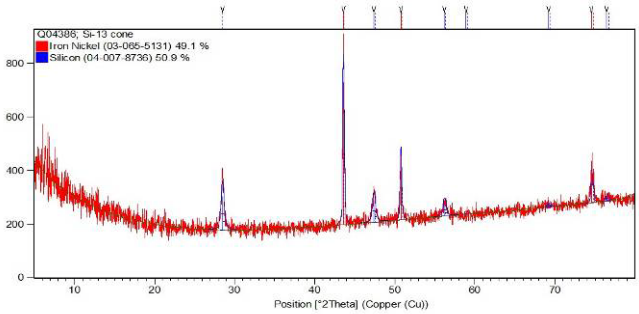

Particle XRD determined composition 50.9% Si, 49.1% Iron-Nickel

Fig. 3.11. SEM and XRD results for Si-13.

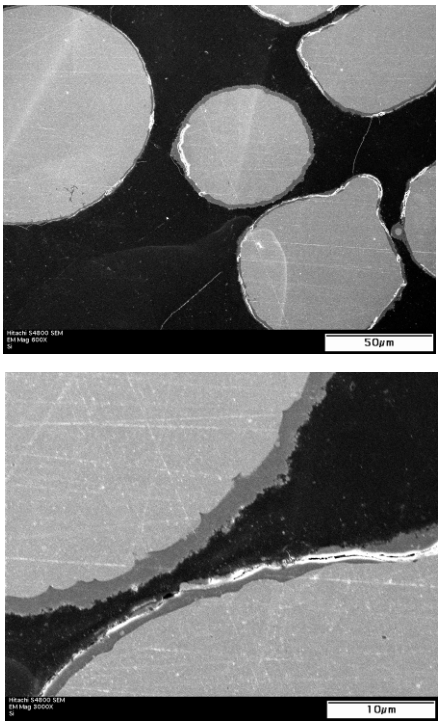

Si-14, 580°C, 2000 sccm TGF, 0.6 % SiH_4

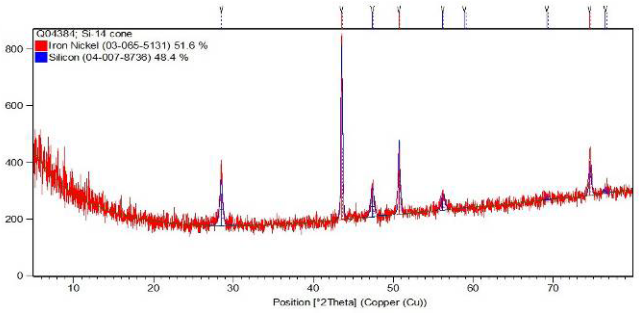

Particle XRD determined composition 48.4% Si, 51.6% Iron-Nickel

Fig. 3.12. SEM and XRD results for Si-14

4. STUDIES PLANNED FOR FY 2010

The work plan for FY 2010 has been approved by the program office at INL. Areas of study are presented in Table 4.1.

Table 4.1. ORNL activities scheduled for FY 2010

Subtask	Comments
Policy decisions	There has been little communication directly between HFIR staff and Office of Science Staff. It is anticipated that at least one meeting will be required to inform SC staff of work conducted at HFIR over the past four years. Likely several interested parties both inside and outside ORNL will wish to participate in this discussion. The HFIR staff believes that several policy issues — enumerated in ref. 10 of this report — must be understood by all participants in the conversion of HFIR.
Quality assurance operations outside HFIR site	Quality assurance for the reactor fuel is a joint responsibility of the reactor owner and the fuel vendor. The reactor owner is responsible for approving the quality assurance plans of the fuel vendor and for auditing the vendor to ensure that the plans are followed. Facilities outside the HFIR site include LANL, Y-12, and BWXT Lynchburg.
Neutronics/thermal hydraulics	ORNL has developed a reference, LEU U-10/Mo fuel design that is believed to be feasible provided adequate fuel qualification data are supplied. This design requires radial and axial grading. Current HEU fuel is only graded in the radial direction, not the axial direction. The HFIR staff believes that with additional analyses using state-of-the-art methods, the requirement for axial grading could be removed.
Oregon State University test loop participation	OSU has stated that their loop could be engineered to provide electrical heating of the fuel. It is likely that this will be required but more study/assessment is needed. This task will include the following: (1) Investigate/review/describe tests related to hydraulics and thermal hydraulics that were done for HFIR for HEU fuel. Document the configuration of the experimental apparatus used for HEU fuel and provide a brief summary of measurements taken. (2) Receive description of LEU fuel plates from neutronics/thermal hydraulics task. (3) Discuss which data from 1) are still applicable and which are not. (4) If some data are not applicable and thus new tests needed, develop a test plan. Define conditions in experiments, how many tests should be done, what should be measured.
Materials science support	To provide support to the fuel development task led by INL.
Operation at 100 MW: (1) fuel qualification tests for LEU fuel	In cooperation with staff at INL and LANL, HFIR staff will prepare a report on HFIR fuel qualification identifying measurements needed to support operations and safety analyses and development of an LEU fuel specification.
Operation at 100 MW: (2) infrastructure upgrades/ analyses to achieve 100MW	HFIR staff will identify components of the reactor plant and infrastructure that are impacted by an increase in operating power; assess level of effort needed to upgrade and certify these elements and develop a preliminary schedule for implementation

5.0 REFERENCES

1. R. T. Primm III, D. Chandler, G. Ilas, B. C. Jolly, J. H. Miller, and J. D. Sease, *Design Study for a Low-Enriched Uranium Core for the High Flux Isotope Reactor, Annual Report for FY 2008*, ORNL/TM-2009/87, March 2009.
2. H. A. McLain, *HFIR Fuel Element Steady State Heat Transfer Analysis, Revised Version*, ORNL/TM-1904, Oak Ridge National Laboratory, Oak Ridge, Tennessee, December 1967 as appended by T. E. Cole, L. F. Parsly, and W. E. Thomas, Revisions to the HFIR Steady State Heat Transfer Analysis Code, ORNL/CF-85/68, April 7, 1986.
3. G. Ilas and R. T. Primm, III, *Fuel Grading Study on a Low-Enriched Uranium Fuel Design for the High Flux Isotope Reactor*, ORNL/TM-2009/223, November 2009.
4. ORNL internal documentation, HFIR-SS-601, HFIR CORE COMPONENTS, RRD-FE-3, REV. 3.
5. J. D. Sease, R. T. Primm III, and J. H. Miller, *Conceptual Process for the Manufacture of Low-enriched Uranium/Molybdenum Fuel for the High Flux Isotope Reactor*, ORNL/TM-2007/39, September 2007.
6. D. Chandler, R. T. Primm, III, and G. I. Maldonado, *Validating MCNP for LEU Fuel Design via Power Distribution Comparisons*, ORNL/TM-2008/126, November 2008.
7. D. Chandler, R. T. Primm, III, and G. I. Maldonado, *Validation of a Monte Carlo Based Depletion Methodology with HFIR Post-Irradiation Examination Data*, ORNL/TM-2009/123, July 2009.
8. Lee Tschaepe, Arthur E. Ruggles, James D. Freels, and R. T. Primm, III, *Evaluation of HFIR LEU Fuel Using the COMSOL Multiphysics Platform*, ORNL/TM-2008/188, March 2009.
9. J. D. Freels, Rao V. Arimilli, Kirk T. Lowe, and Isaac T, Brody, *The Role of COMSOL Toward a Low-Enriched Uranium Fuel Design for the High Flux Isotope Reactor*. Proceedings of the 2009 COMSOL Conference, CD, Boston, Ms, October 9-10, 2009.
10. Tracey Guida and R. T. Primm, III, *Establishing a Cost Basis for Converting the High Flux Isotope Reactor from High Enriched to Low Enriched Uranium Fuel*, ORNL/TM-2009/311, February 2010.
11. D. M. Wachs, *RERTR Fuel Development Plan*, INL/EXT-05-01017, Rev. 4, August 27, 2009.

APPENDIX A

THE ROLE OF COMSOL TOWARD A LOW-ENRICHED URANIUM FUEL DESIGN FOR THE HIGH FLUX ISOTOPE REACTOR

Abstract Design and safety analyses are underway to convert the High Flux Isotope Reactor (HFIR) at the Oak Ridge National Laboratory (ORNL) from a high-enriched uranium (HEU) fuel to a low-enriched uranium (LEU) fuel. The primary constraint for the project is that the overall fuel plate dimensions and the current neutron flux performance must remain unchanged. This allows minimal impact on the facility and cost for the conversion, and provides transparency to the HFIR customer base and research projects that depend on the facility for isotopes and neutron flux. As a consequence, the LEU design demands more accuracy and increased definition and focus on safety margin in the analysis efforts than the original design.

Several technical disciplines are required to complete this conversion including nuclear reactor physics, heat transfer, fluid dynamics, structural mechanics, fuel fabrication, and engineering design. The role of COMSOL is to provide the fully-coupled 3D multi-physics analysis for heat transfer, turbulent flow, and structural mechanics of the fuel plates and flow channels. A goal is for COMSOL to simulate the entire fuel element array of fuel plates (171 inner, 369 outer). This paper describes the progress that has been made toward development of benchmark validation models of the existing HEU inner-element fuel plates.

Keywords nuclear fuel, heat transfer, fluid flow, structural mechanics, COMSOL

Research funded by the Department of Energy (DOE) Office of Science and the Global Threat Reduction Initiative (GTRI) of the National Nuclear Security Administration (NNSA) http://nnsa.energy.gov/news/2330.htm

James D. Freels, Ph.D.
Oak Ridge National Laboratory
1 Bethel Valley Road
P.O. Box 2008
Oak Ridge, TN 37831-6392
Office: (865)576-8645
Fax: (865)241-2712
E-mail: freelsjd@ornl.gov

Rao V. Arimilli, Professor · Kirk T. Lowe · Issac T. Bodey
The University of Tennessee
Mechanical, Aerospace, and Biomedical Engineering Department
1512 Middle Drive
235 Dougherty Engineering Building
Knoxville, TN 37996-2030
Office: (865)974-5300
Fax: (865)974-5274
E-mail: arimilli@utk.edu

1 Research Goals

A primary constraint on HFIR operations is the thermal limit obtained from design and safety analyses. The present limitations at a power level of 85Mw using HEU fuel is based on steady-state analysis using the SSHTC [1] code and transient analysis using the RELAP5 [2] code. RELAP5 remains under active maintenance by the NRC and DOE (depending on which version used) and the HFIR facility will update their RELAP5 models when the LEU design is committed. The current set of calculations that provide the RELAP5 portion of the safety basis will likely require repeating. Much of the input into the RELAP5 models depends directly on the results from the design-based SSHTC.

The SSHTC code was developed at the time HFIR was originally designed and constructed in the mid-1960s and has changed very little since. The basis for the thermal limits include a strong validation history of testing and experiments. The HFIR has operated safely since approximately 1966 and is now on HEU fuel cycle #423 (about 6-10 cycles per year) and counting. The code documentation and design/structure are not convenient for changing the code to accommodate an LEU design change; i.e., classic '60s vintage FORTRAN along with difficult documentation and few embedded code comments. Further, in order to meet the design goal of achieving an equivalent neutron flux performance within the same overall external dimensions, the analysis must be carried out well beyond the capabilities of the present SSHTC code. Therefore, in order to perform an equivalent design and safety analysis for LEU fuel using the legacy codes, a major code development effort would be required if the SSHTC were to be retained as the basis code.

The major item of analysis improvement required to achieve a new HFIR LEU design is a significant reduction

in the "hot spot factor" (HSF). The HSF is a direct accounting for the uncertainty in manufacturing tolerances and defects such that a reduction in heat transfer capability (increase in thermal resistance) occurs. The resulting increase in temperature causes a reduction in the safety margin and therefore restricts the operating range of HFIR. Based on present 1-D SSHTC analysis, the hot spot is verified to be acceptable by X-ray scanning during the manufacturing process if the defect area is less than approximately 0.25-inch square.

This same HSF is also used in the 1-D transient analysis carried out by RELAP5. The HSF is implemented in RELAP5 by modeling a separate host spot area, and imposing a power distribution increased by the HSF. Several hot spots are modeled in this manner with the worst case being at the core exit. A "hot streak" is also modeled in RELAP5 in a similar manner.

The application of the HSF is made in a single direction normal to the fuel plate; also the same direction as the main convection between the plate and the coolant. The dominant mode of heat transfer by conduction in the fuel plate is not credited in the other two dimensions. In utilizing a modern analysis code, such as COMSOL, on this problem, heat transfer by conduction and convection is accounted for in all three directions of space. Furthermore, additional physics are also fully coupled to the problem in full detail including structural mechanics. It is expected that the enhanced analysis will significantly reduce the HSF and a companion increase in the margin of safety. It may also be possible to improve the performance level of the HFIR.

The essential research goals are:

- Validate COMSOL results for the existing HEU fuel plate in pseudo-1D/2D against the SSHTC and companion test/experiment data taken during the era of the HFIR core design,
- Develop a detailed, realistic 3D COMSOL model of a single HEU fuel plate and coolant channel for flow, heat transfer, and structural mechanics coupled multiphysics, and demonstrate the improvement in HSF and safety margin, and
- Develop a companion LEU fuel-plate model (significantly different internals) at the proposed 100 Mw power level and compare performance. It is anticipated that a test program will be conducted to validate the LEU model results.

It is also proposed that an "enhanced HEU" HFIR core will be tested to demonstrate the improved safety margin realized prior to testing of an LEU-fueled HFIR core.

2 Tasks Currently Underway or Identified

An entry-level study[3] was conducted by a separate research group to evaluate the fundamental capabilities of COMSOL on this problem. The results were only marginally acceptable; primarily due to the inexperience of the researchers in using COMSOL causing many fundamental flaws in the analysis.

A new research team has been formed composed of individuals with extensive COMSOL experience. The first task of this team has been to check and review the initial findings. This work is approaching the completion stage and will result in a revised or new report. The tasks nearing completion are:

- verify the models and results from the prior report,
- document and verify SSHTC inputs required for input into COMSOL,
- verify finite-element accuracy by energy-norm methods as compared to graphical solution results,
- develop a COMSOL material library for HFIR-specific materials including water that is temperature and pressure dependent,
- develop a 2D non-isothermal turbulent model of the HFIR HEU fuel plate,
- verify proper boundary conditions to be used in the modeling with particular attention to the entrance and exit regions,
- develop a COMSOL-fitted nuclear fuel power distribution curve and verify proper integrated power levels, and
- overlay COMSOL results against SSHTC results.

After completion of these tasks, several additional tasks are to be completed while still focused in the 2D solution mode. These tasks include

- developing proper boundary layer meshing and determine valid ranges for y^+ and T^+ mesh dependence,
- investigate options for turbulent Prandtl number provided by COMSOL,
- develop a consistent local hot-spot model revision,
- develop a consistent entrance and exit model revision,
- accommodate a fitted-curve power distribution function provided by separate nuclear physics calculation, and
- compare and document the final, best-estimate 2D representation generated by COMSOL against equivalent SSHTC and/or RELAP5 results.

The lessons learned from these 2D studies are directly applicable to the 3D models. An efficient transition to the much more complex and computationally-intensive 3D extension can be achieved with minimal waste with this type of geometric representation of a HFIR fuel plate. For example, the near-wall mesh requirements will have been established, all the material-property libraries developed, and power distribution methodology verified. Four additional areas of development have been identified and started in the 3D framework:

- development of 3D geometry and meshing extruded from a 2D working plane,
- in parallel, develop the 3D geometry with *Solidworks* and generate the mesh with COMSOL using the "live

connection" capabilities of the two codes (early results with this approach show the additional benefit of a reduced number of surfaces to specify for boundary conditions),
- application of consistent boundary conditions upon the increased number of surfaces now present in the 3D model; including the application of extrusion coupling to provide for symmetry to the coolant channel, and
- development of the 3D iterative solution methods required to obtain a converged steady-state solution within the computing environment.

These 3D tasks are well underway and some preliminary results are presented here and in the conference presentation material.

3 Areas of Intense Focus

The HFIR fuel plate is designed with a very thin (0.050-inch) thickness across which is the predominant direction of heat transfer by convection from the nuclear-heated fuel to the coolant. In the span-wise direction, the scale is a few inches (3.6" for the inner element, and 3.2" for the outer). The length-wise direction, which is the predominant direction of the coolant flow, is 24-inches. Therefore, the aspect ratio is $\sim 74-72$ in the span-wise direction and ~ 480 in the length-wise direction. To compound the situation, because the Reynolds number, based on the channel width, is approaching 10^5, a fine mesh is required near the wall in the coolant region in order to capture the turbulent boundary layer profile and produce a reasonable y^+ range. Therefore, the aspect ratio demands on the finite elements are extremely large in the length-wise direction in order to be able to obtain a solution. Fortunately, experience has shown that because the flow is dominant in the length-wise direction, large aspect ratios are acceptable for consistent solutions. Therefore, even though the COMSOL mesh generation tools will show a poor quality element resulting from these large aspect ratios, a careful study of the axial (or length-wise) mesh spacing caused by the mesh extrusion process should reveal solutions consistent with the available test data. Hence, a primary research focus is the maximum acceptable mesh spacing in the axial direction.

The HFIR was designed to provide the highest neutron flux in the world for the production of neutrons and isotopes. As a consequence, the demands for heat flux management are high, hence, the high Reynolds number flow mentioned earlier. Therefore, it is possible that the range of applicability of the COMSOL turbulence models provided by the heat transfer and/or chemical-engineering application modes; i.e., $k-\varepsilon$ and $k-\omega$, may be deficient in accuracy for this range of heat and momentum flux. If this turns out to be the case, COMSOL provides the tools to be able to modify these models by either a better model obtained from literature and/or industry or by derivation of a new model. Hence, another primary area of research focus is on the accuracy and proper application of the given turbulent models and changing these models should it become necessary.

Early results from the 3D model solutions have found that a single fuel plate and adjacent coolant channel can be solved with a reasonable level of accuracy with about 100 axial mesh spacings yielding approximately 5×10^6 degrees of freedom (to be solved). The resulting multigrid-based iterative solution method requires about 40 GB of memory and takes about a cpu-week to solve on a single 8-core, shared memory, dual-processor, 64-bit AMD cluster node. We are interested in solving the entire HFIR core which consists of 171 inner fuel plates and 369 outer fuel plates. Needless to say, we are most interested in the potential gains to be obtained from the upcoming release of the COMSOL distributed parallel processing. We expect this to be a difficult goal to achieve and will occupy much of our research focus.

4 Current Status and Results

2D Results

The 2-D, vertical cross-section, non-isothermal HEU fuel plate model exhibits a strong dependence on the chosen meshing scheme. The mesh must be sufficiently dense at the solid-fluid boundary in order to produce the required range of y^+ for the turbulent boundary layer simulation. Our first approach was to utilize the free mesh (FM) capabilities of COMSOL for all domains in the geometry. A quality analysis of the model revealed large relative errors in the energy balance of the fluid domain, while the energy balance in the solid retained very good agreement, on the order of 1×10^{-3}%. The large errors in the fluid domain were obtained regardless of the number of mesh refinements conducted. Utilizing the COMSOL adaptive mesh feature brought no improvement in this error.

Mapped meshes (MM) are recommended by COMSOL for thin structures such as the HFIR fuel plate. The mesh was changed to a MM approach for those regions that did not involve a curvature in the geometry. This change allowed a suitable mesh to be generated in the fluid domain adjacent to the fuel plate. Also, the number of elements decreased significantly with the MM relative to the FM. While the mesh was visually acceptable in terms of sufficient density at the solid-fluid boundary, the large relative error in the energy balance of the fluid remained.

A boundary layer meshing (BLM) approach was then investigated. One advantage of the BLM is suitability along the curved leading edge of the fuel plate. With minimal refinements, the large relative error in the energy balance of the fluid was reduced below 4%. The trade off for this acceptable model quality is the increase in CPU time and RAM consumption. While the number of elements ($\sim 2 \times 10^5$) in the BLM was less than the FM, the total degrees of freedom was still significant at $\sim 2 \times 10^6$

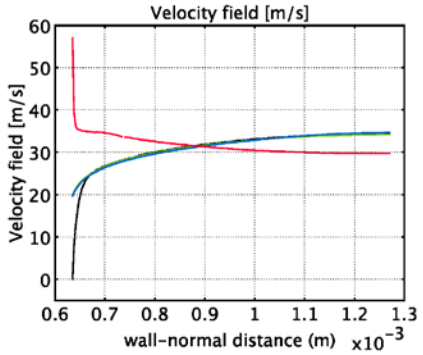

Fig. 1 Preliminary 2D Results: Velocity Profiles at flow channel entrance (red), start of heated section (blue), end of heated section (green), and exit of the flow channel (black).

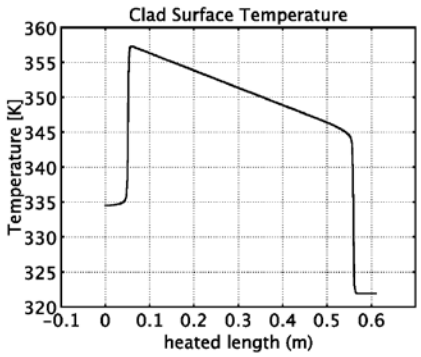

Fig. 2 Preliminary 2D Results: Clad surface temperature along the turbulent flow wall interface. Note: left to right indicates exit to entrance of the flow channel.

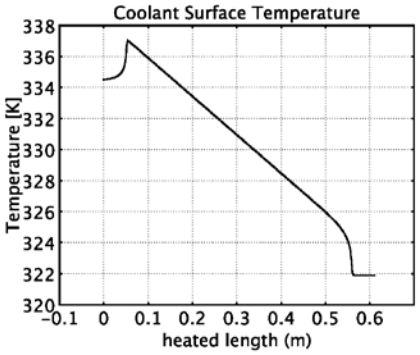

Fig. 3 Preliminary 2D Results: Coolant surface temperature along the turbulent flow wall interface. Note: left to right indicates exit to entrance of the flow channel.

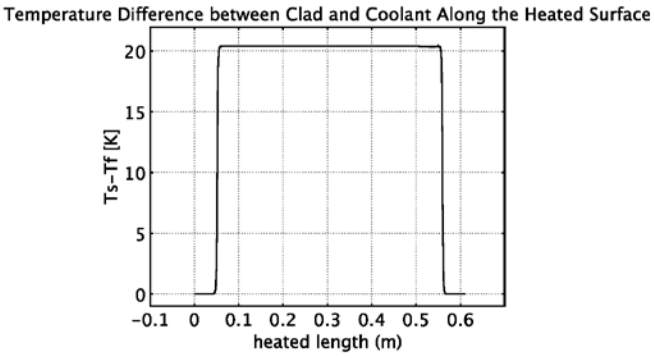

Fig. 4 Preliminary 2D Results: Clad-Coolant Temperature difference along the turbulent flow wall interface. Note: left to right indicates exit to entrance of the flow channel.

Some preliminary 2D results in Figure 1 demonstrate the classic development of the turbulent boundary layer profile in the coolant channel. The high Reynolds number and narrow channel width is apparent.

Close examination of the temperature profile at the solid and fluid interface is shown by Figures 2 through 4 inclusive. The coolant entrance is at ~ 0.6096 meters (24 inches) above the core exit and temperature increasing toward the exit (left). A near constant temperature difference of ~ 20K is shown in Figure 4.

A typical 2D result obtained in an earlier study of the total temperature of the fuel and coolant system overlayed with velocity contours is shown by Figure 5 demonstrating the importance of the entrance and exit effects on the velocity. Note that the velocity contours are of non-zero slope at the exit which implies that not all the convection heat transfer is complete in the system as it is currently modeled. The dominant mode of heat transfer is by convection in the wall-normal direction perpendicular to the coolant flow direction. However, since the goal is to credit all heat transfer mechanisms in this system, we anticipate an extension in the exit flow recovery length just as the actual HFIR core is designed.

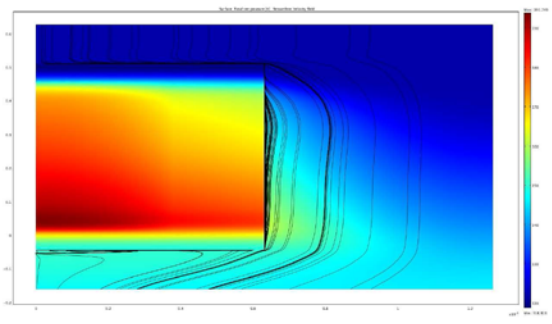

Fig. 5 Preliminary 2D Results: Total temperature overlayed by constant-velocity contour lines.

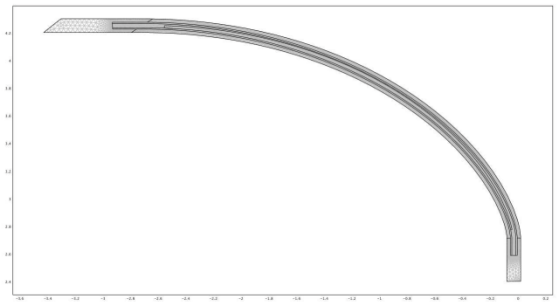

Fig. 6 COMSOL Cross Section Meshing of the HFIR Inner Fuel Element.

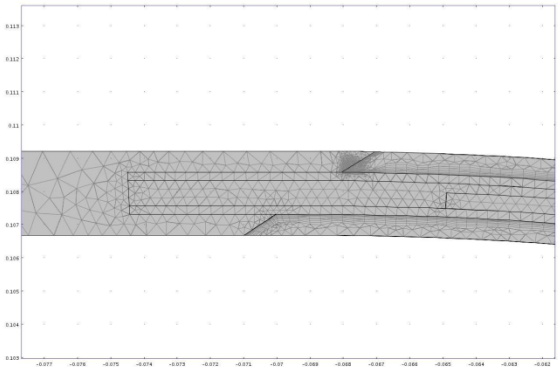

Fig. 7 Mesh Details of the HFIR Inner Fuel Plate COMSOL Model.

3D Results

The geometry of the HFIR fuel plates is an involute shape. This basic shape and fuel internals are modeled with COMSOL tools to yield the following mesh as shown in Figure 6.

A closeup of the meshing details showing the side plates, coolant, clad, filler, and fuel regions is in Figure 7. Troublesome areas near the coolant corners required extra mesh density to resolve.

This cross-section mesh was then extruded in the axial (z) direction to provide a full 3D simulation of the fuel plate and adjacent cooling channel. The computational requirements are extensive due to the large aspect ratio of the actual geometry (24" high , 0.050" fuel plate thickness) and the boundary layer mesh requirements of the variable-density Navier-Stokes equations.

Figure 8 shows the boundary segments used to produce the outer limits of the fuel plate and flow channel.

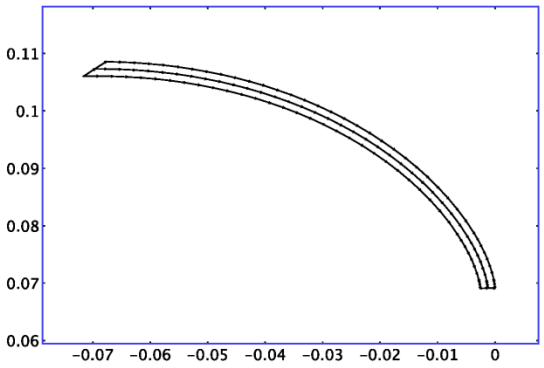

Fig. 8 COMSOL Boundary Elements of the HFIR Inner Fuel Element.

The number of boundary elements is determined by the construction method, i.e. constant arc length or constant angle between construction points. This type of geometry construction results in at least 126 boundaries. Even more boundaries or construction points would be needed to refine the curvature of the involute. In contrast, a similar Solidworks model would result in only 11 boundaries because each face is imported as a boundary.

Constructing the 3D model in Solidworks provides a straight-forward implementation of boundary conditions. However, more effort is required upfront to construct and repair the CAD model so that it will mesh successfully. In the draw mode, the imported geometry may look disjointed, but applying a mesh will refine the curvature in COMSOL so that it better resembles the initial solid model. Once meshing is completed, the assignment of boundary conditions and extrusion coupling variables is greatly simplified.

A typical result of the simulation is shown in Figure 9 for the metal surfaces. This model solves the non-isothermal form of the Navier-Stokes equations, along with the $k-\varepsilon$ turbulence model. This set of equations results in 8 independent variables $(u, v, w, p, logk, logd, Ts, Tf)$ to be simultaneously solved in 3D steady-state. The present model utilizes a geometry without the entrance and exit regions (the importance of which was demonstrated in Figure 5), and creates the 3D mesh by simple extrusion of the working-plane mesh shown in Figures 6 and 7. The most-detailed axial spacing solved thus far using this simple extrusion method was 96 elements ($\frac{1}{4}$-inch spacing) using linear-basis elements for all the variables and resulted in approximately 5×10^6 degrees of freedom to be solved. Even at this resolution, it is not clear that a sufficient level of mesh refinement (particularly in the axial, or length-wise, direction) is sufficient for this model (to be determined).

Even on our 64-bit AMD64 computer with 64GB of memory, this model is prohibitively large to be solved using the COMSOL direct solvers. Therefore, the recommended approach, based on the GMRES iterative solver, is

utilized. The problem is first split into three groups by using the segregated stationary solver (u,v,w,p) , $(logk,logd)$, (Ts,Tf). Each group uses the GMRES iterative solver with the multigrid preconditioner. The multigrid meshing is set up manually by creating, and saving the mesh to file, mesh spacings of 12, 24, 48, and 96 axial elements and naming the sets mesh case 4, 3, 2, and 1 respectively. Mesh case 0 is identical to mesh case 1 with the element basis increased to quadratic everywhere (but has not been solved yet).

Within each preconditioner iteration, all mesh cases are both used and assembled. 4 outer preconditioner iterations are performed using the V-cycle multigrid cycle. For all the segregated set, a blocked SOR presmoother is performed at 4 iterations and a relaxation factor of 0.8. The postsmoother is set up identically as the presmoother. The coarse solver is solved directly using the PARDISO solver (mesh case 4).

Within each segregated step, a constant damping factor is set at 0.5 and 2-3 iterations are performed with minimal Jacobian update. The iterations are stopped at either step numbers 2-3 or tolerance of 1.0×10^{-2}. The overall convergence criteria for each segregated step was set at 1.0×10^{-4}.

With these settings, the model took about a week of clock time to converge using 8 cpu shared-memory processors on a 64-bit AMD64 Debian/Gnu-Linux machine using version 3.5 of COMSOL. The memory required was about 40 GB of the 64 GB available during this time. On average, about 6 load factor was constantly used indicating only 75% utilization of the processors available. The model could be stopped and restarted, and the new plot while solving feature was nice. We have not tried version 3.5a, having the new SOR enhancements, on this problem yet, but hope to do this soon. Our main goal was to demonstrate that we could solve the problem in a reasonable time frame and obtain a meaningful solution. We anxiously anticipate further improvements in solution time with the distributed parallel processing capabilities of COMSOL to be released soon.

5 Conclusions

It is early in the COMSOL model development for this project, but these preliminary simulations look very promising. The challenge will be to determine the number of axial mesh levels and boundary layer resolution such that a good match with early test data on the fuel design is sufficiently matched. With confidence gained from validation of the HEU fuel simulations, extended simulations of the LEU fuel redesign will be forthcoming.

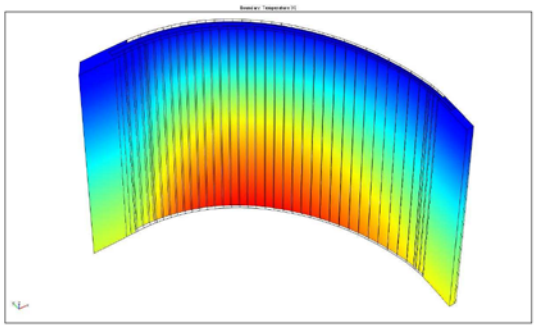

Fig. 9 Metal Surface (non-coolant) Temperature for a Typical COMSOL Simulation of a HFIR Inner Fuel Plate.

References

1. McLain, H. A., "HFIR fuel element steady state heat transfer analysis: revised version," Tech. Rep. ORNL/TM/1904, Oak Ridge National Laboratory, 1967.
2. Morris, D. G. and Wendel, M. W., "High Flux Isotope Reactor System RELAP5 Input Model," Tech. Rep. ORNL/TM-11647, Oak Ridge National Laboratory, 1993.
3. Tschaepe, L., Reuggles, A. E., Freels, J. D., and Primm III, R. T., "Evaluation of HFIR LEU Fuel Using the COMSOL Multiphysics Platform," Tech. Rep. ORNL/TM-2008/188, Oak Ridge National Laboratory, 2008.

APPENDIX B

STATISTICAL CONSIDERATIONS IN THE DETERMINATION OF THE ADEQUATE NUMBER OF IRRADIATION TESTS

"There are known knowns. These are things we know that we know. There are known unknowns. That is to say, there are things that we know we don't know. But there are also unknown unknowns. There are things we don't know we don't know. So when we do the best we can and we pull all this information together, and we then say well that's basically what we see as the situation, that is really only the known knowns and the known unknowns."

Secretary of Defense, Donald Rumsfeld, June 6, 2002.

While it is the responsibility of the INL to qualify the LEU fuel for use in U.S. high performance reactors, it is the responsibility of the operating contractor for HFIR to determine if the qualification tests conducted by INL are adequate for HFIR and the responsibility of the Department of Energy Office of Science to concur or not concur with the judgment of the HFIR operating contractor. The INL experimental program is documented in ref. 11. The studies reported here are a first attempt to determine the number of tests needed to be confident that the fuel plates will meet defined standards. Given that the responsibility of the GTRI program to HFIR extends only through the irradiation of the first LEU core, the goal of these studies is to have the plates fail less than 1 in every 540 times (there are 540 plates in a HFIR assembly). To determine the adequacy of the proposed irradiation experiments, we need to consider four different components: the confidence level, the power, the standard deviation, and the margin of error.

The confidence level is a measure of the reliability of the calculation; it is expressed as a percentage and indicates how often the conclusions derived from consideration of our sample will agree with the true population. By choosing the confidence level we wish to attain we can predict the degree of reliability of our research. Using above a 95% confidence level is usually sufficient. A Z-score is the parameter that corresponds to the number of standard deviations a particular value varies from the mean. After determining our confidence level, we can find the corresponding z-score value using the statistics table provided in Table B.1.

Table B.1. Z-scores for a 2-sided calculation

Confidence Level	Z_α
99.9%	3.2908
99%	2.5762
95%*	1.9604
90%	1.6452
85%	1.4398
80%	1.2817
75%	1.1504
70%	1.0364
68.3%	1.0000
65%	0.9345
60%	0.8415
55%	0.7552

Our reliability is also determined by the statistical power of our calculations. Power is our ability, in this case, to detect a faulty plate if it exists. A power level is the probability that a test will not make a type II statistical error, i.e. the test will not produce a false negative result. Using a power above 80% is usually sufficient. After determining our power level, we can find the corresponding z-score value using the statistics table provided in Table B.2.

Table B.2. Z-scores for selected power values

Power level	Z_{β}
70%	0.53
80%*	0.84
90%	1.28
95%	1.64
97.5%	1.960
99%	2.326

Note: It is conventional to use at least 80% power and a 95% confidence level

Each parameter that needs to be tested with regard to the fuel has its own measurement standard deviation and design basis margin of error. The standard deviation is associated with the measurement technique used to determine the value of the parameter. It describes the variation in *measurement* about the sample mean and, therefore, the population mean. A large relative standard deviation will lead to a requirement for a large number of tests (sample size) to be conducted in order for the sample set to be representative of the population. Process parameters and standard deviations for measurement techniques for those parameters were obtained the production of the current, HEU fuel as well as expert opinion and are shown in Table B.3.

The margin of error is the *design tolerance* for the parameter; the range in which the value of the parameter can vary from the nominal value and be accepted for use in the reactor. A large design tolerance will lead to the requirement for a large sample size for a given confidence value, as more variability will require a higher number of tests (sample size) to be conducted. The margin of error values are shown in Table B.4 and were obtained from current, HEU fuel specifications where appropriate and otherwise from expert opinion. Data for LEU fuel do not currently exist for all the parameters noted in Tables B.3 and B.4 though a minimal amount of data for fuel foil thickness are available and are shown in Table B.5.

The following formula (eq. B.1) comes from Ref. B.1. The author of that reference, Cochran, was a statistician during the early-mid 1900's and has made several notable contributions to the field of statistics. Much of his work included experimental design, analysis and observational studies. The formula we will be applying "uses two key factors: (1) the risk the researcher is willing to accept in the study, commonly called the margin of error, or the error the researcher is willing to accept (in this study, the design basis tolerance for a parameter), and (2) … the level of acceptable risk the researcher is willing to accept that the true margin of error exceeds the acceptable margin of error (otherwise known as our confidence level)" (Ref. B.2). This formula is designed to test sets of continuous data, i.e., data that has specific values, and not solely categorical labels. Additional information regarding this statistical technique and definitions of statistical parameters can be found in Ref. B.3 through B.5. Examples of the use of the formula are found in Appendix C.

$$N = \frac{\left(Z_\alpha + Z_\beta\right)^2 * s^2}{E^2} \qquad \text{(Eq. B.1)}$$

N = sample size
Z = the Z-statistical value
Z_α = the Z-Statistical value relating to our level of Confidence
Z_β = the Z-statistical value relating to our level of Power
s = standard deviation
E = margin of acceptable error

Using data from Tables B.3 and B.4 and applying Eq. B.1, then number of tests (number of plates) needed to be fabricated for HFIR fuel is shown in Table B.6. Obviously at higher confidence levels and powers, it is necessary to test more fuel samples. Note that zero (0) is a numerical artifact and that one plate would always be the minimum number tested.

Most of the parameters from Tables B.3 and B.4 have relatively small standard deviations with respect to their margin of error. This results in very few plates needing to be tested. Due to the laws of normal distribution, 99.7% of the results will fall within three standard deviations of the mean. Thus, as long as the margin of error is three times greater than the standard deviation, few tests need to be completed. This is the case for all of the parameters with known values, except for "Assembled plate thickness." This parameter has a margin of error that is much smaller than the standard deviation, which results in an increased number of tests. Requiring a higher confidence level and power increases the number of tests to be completed. For example, at the extremely reliable and precise 99.9% confidence and 99% power, this parameter requires 3056 tests to be completed. But, if confidence is dropped to 95% and power to 80%, which are the two conventional values for these components, the number of tests decreases to 760, an almost 75% decrease.

For the parameters with unknown standard deviations and/or margins of error (present in LEU/Mo foil plate design but not in the current, HEU plate), a sensitivity study was conducted. The study compared the ratio of a standard deviation to a margin of error. In the case that the standard deviation was less than the margin of error, tests were conducted at varying confidence and power levels. Results are shown in Tables B.7

As the margin of error became several times larger than the standard deviation, the number of tests needed to be conducted approached zero. Similarly, in the case that the standard deviation was greater than the margin of error, tests were conducted at varying confidence and power levels. It can be noted that as the standard deviation became several times larger than the margin of error, the number of tests needed to be conducted approached infinity.

The practical aspect of the cases in Table B.7 is to emphasize the importance of measurement techniques for process parameters for LEU fuel. The limited irradiation test program scheduled for INL mandates that very accurate and precise measurement techniques be developed for all process variables important to quality assurance of the fuel. A ratio of design tolerance-to-standard deviation of measurement technique of five seems to be required.

Table B.3. Standard deviations for measurement techniques for parameters important to the manufacture of LEU fuel

Parameter to be measured	Expected value	Standard deviation (same units as expected value)		Assumed measurement technique
		Absolute	Relative (std. dev./ mean)	
Weight of fuel foil	?	?	10^{-5}	Scale
Length zone 1	5.11 cm	0.025		Real time radiography
Length zone 2	4.46 cm	0.05		
Length zone 3	49.49	0.05		
Length zone 4	5.11 cm	0.05		
Length zone 5	4.46 cm	0.05		
Left margin U/Mo zone 1	>0.432 cm	0.025		
Left margin U/Mo zone 2	0.770 cm	0.025		
Left margin U/Mo zone 3	0.505 cm	0.025		
Left margin U/Mo zone 4	0.770 cm	0.025		
Left margin U/Mo zone 5	>0.432 cm	0.025		
Right margin U/Mo zone 1	>0.533 cm	0.025		
Right margin U/Mo zone 2	0.871 cm	0.025		
Right margin U/Mo zone 3	0.613 cm	0.025		
Right margin U/Mo zone 4	0.871 cm	0.025		
Right margin U/Mo zone 5	>0.533 cm	0.025		
Thickness of U/Mo	various	-	0.12	Modified homogeneity scanner
Mo content	0.1 g Mo/g	0.001		Chemical separation?
Wt. fraction U-235	0.1975	0.001		Mass spectrometry
Density of U/Mo	17.02 g/cm^3	0.001		Weight/volume
Trace elements boron equivalent	0.1 mg/g U	-	.01	Various
Boron loading in plate	10 g	0.05		Analysis from manufacturer
Maximum non-bond size (fuel to Zr)	0.02 cm^2	?		Unknown; consider multipliers on margin of error, 1, 0.5,0.1,0.01
Maximum non-bond size (Zr to Al)	0.02 cm^2	?		Unknown; consider multipliers on margin of error, 1, 0.5,0.1,0.01
Zircaloy thickness above U/Mo	25 microns	-	0.10	Modified homogeneity scanner with correlated measurement to U/Mo
Zircaloy thickness below U/Mo	25 microns	-	0.10	Modified homogeneity scanner with correlated measurement to U/Mo
Zr length beyond U/Mo top	0.254 cm	0.025		New, tunable, real time radiography
Zr length beyond U/Mo top	0.254 cm	0.025		New, tunable, real time radiography
Zr Left margin U/Mo zone	0.254 cm	0.025		New, tunable, real time radiography
Zr Left margin U/Mo zone	0.254 cm	0.025		New, tunable, real time radiography
Assembled plate thickness	0.127 cm	0.025		Current practice

Table B.4. Margin of error (design tolerance) for measured parameters

Parameter to be measured	Expected value	Absolute margin U/Mo of error in design (∀ assumed equal unless otherwise specified)
Weight of fuel foil	?	0.004 (relative margin)
Length zone 1	5.11 cm	0.635 cm
Length zone 2	4.46 cm	0.635 cm
Length zone 3	49.49	4.460 cm
Length zone 4	5.11 cm	0.635 cm
Length zone 5	4.46 cm	0.635 cm
Left margin U/Mo zone 1	>0.432 cm	-
Left margin U/Mo zone 2	0.770 cm	0.338 cm
Left margin U/Mo zone 3	0.505 cm	0.074 cm
Left margin U/Mo zone 4	0.770 cm	0.338 cm
Left margin U/Mo zone 5	>0.432 cm	-
Right margin U/Mo zone 1	>0.533 cm	-
Right margin U/Mo zone 2	0.871 cm	0.338 cm
Right margin U/Mo zone 3	0.613 cm	0.080 cm
Right margin U/Mo zone 4	0.871 cm	0.338 cm
Right margin U/Mo zone 5	>0.533 cm	-
Thickness of U/Mo	various	12 microns
Mo content	0.1 g Mo/g	0.01 g Mo/g
Wt. fraction U-235	0.1975	0.001
Density of U/Mo	17.02 g/cm^3	0.17 g/cm^3
Trace elements boron equivalent	0.1 mg/g U	0.01 g U
Boron loading in plate	10 g	0.1 g
Maximum non-bond size measurement (U/Mo to Zr)	0.02 cm^2	See Table B.3
Maximum non-bond size measurement (Zr to Al)	0.02 cm^2	See Table B.3
Zircaloy thickness above U/Mo	25 microns	5 microns
Zircaloy thickness below U/Mo	25 microns	5 microns
Zr length beyond U/Mo top	0.254 cm	0.05 cm
Zr length beyond U/Mo top	0.254 cm	0.05 cm
Zr Left margin U/Mo zone	0.254 cm	0.05 cm
Zr Left margin U/Mo zone	0.254 cm	0.05 cm
Assembled plate thickness	0.127 cm	0.00254 cm

Table B.5. Thickness measurements for selected foils
(data provided by Y-12 National Security Complex)

ID	wt	Thicknesses, 5 places along length, in mils						length	width	wt of chem sample
INL 3	211g	15.8	15.6	15.6	15.5	15.6		23 9/16"	2 3/32"	9g
Agent X	192g	13.8	13.4	13.5	13.5	13.7		23 9/16"	2 3/32"	10g
Agent Z	191g	13.8	13.6	13.6	13.4	13		23 9/16"	2 3/32"	10g
INL 4-2A	208g	15.6	15.5	15.5	15.6	15.3		23 9/16"	2 3/32"	11g
INL 6	94g	14.6	14.8	14.5	14.4	14.4		23 9/16"	2 3/32"	9g
INL 8-1	204g	14.6	14.7	14.8	14.7	14.7		23 9/16"	2 3/32"	9g
INL 10-1	674g	18.3	18.4	20	18.8	18.7		49"	2.6"	13g
INL 11-3	677g	20	20	20	20	19		49"	2.4"	15g
INL 6-2	835g	18.3	18.3	19	18.2	17.7		49"	3.2"	(already have INL 6)
INL 5-2	769g	17.3	17.8	18	20	19.7		49"	3.161"	10g
INL 4	736g	21	20	21	21	18	18	49"	2.6"	(already have INL 4-2A)
INL 4-2	802g	17.7	17.6	17.5	17.8	17.8		49"	3.2"	(already have INL 4-2A)
INL 16-2	707g	17.4	17.5	17.6	17.5	16.8		49"	2.8"	12g
INL 6	759g	19.3	18.9	17.5	16.9	16.9		49"	3.1"	(already have INL 6)
INL 16-3	627g	15	15	15.3	15.2	15.7		49"	2.8"	(already have INL 16-2)
FSM 12	711g	15.7	17.5	16.8	15.9	15.7		49"	3.0"	(sampled under PDRD)
INL 10-3	670g	15.7	15.9	15.8	16	15.8		49"	3.0"	(already have INL 10-1)
INL 5	715g	16.1	16.3	16.9	18.2	19		49"	2.9"	(already have INL 5-2)
INL 12-1	598g	19.2	18.3	18	18.9	18.8		49"	2.3"	11g
INL 10-2	667g	15.6	16.1	16.1	16.3	15.8		49"	2.9"	(already have INL 10-1)
INL 8b	585g	16.3	16.6	16.8	16.5	17		48 5/8"	2.5"	10g
INL 8a	635g	17.5	17.8	18.3	17.7	17.6		49"	2.5"	11g
INL 9-3	714g	18.1	18.3	19.3	19.3	18.8		49"	2.7"	11g
INL 11-2	561g	16.1	16.4	16.4	16.4	15.9		49"	2.4"	(already have INL 11-3)
INL 9-1	405g	13.4	13.5	13.4	13.3	13.1	bowed	49"	2.13"	(already have INL 9-3)
INL 12-3	489g	15.8	15.6	15	15	15.1		49"	2.2"	(already have INL 12-1)
INL 16-1	514g	13.2	13.1	13.5	14.6	15		49"	2.7"	(already have INL 16-3)
INL 2a	517g	14.8	14.9	15.2	16	15.2		49"	2.3"	10g

Table B.6. Number of plates to be tested for (1/540) failure

Parameter to be measured	Confidence	Z_α	Power	Z_β	$(Z_\alpha + Z_\beta)^2$	s	s^2	E	E^2	# of trials
Weight of fuel foil	99.9%	3.2908	99%	2.326	31.5484	0.00001	0.000000	0.004	0.000016	0
Length zone 1	99.9%	3.2908	99%	2.326	31.5484	0.025	0.000625	0.635	0.403225	0
Length zone 2	99.9%	3.2908	99%	2.326	31.5484	0.05	0.002500	0.635	0.403225	0
Length zone 3	99.9%	3.2908	99%	2.326	31.5484	0.05	0.002500	4.46	19.891600	0
Length zone 4	99.9%	3.2908	99%	2.326	31.5484	0.05	0.002500	0.635	0.403225	0
Length zone 5	99.9%	3.2908	99%	2.326	31.5484	0.05	0.002500	0.635	0.403225	0
Left margin U/Mo zone 1	99.9%	3.2908	99%	2.326	31.5484	0.025	0.000625	-	-	-
Left margin U/Mo zone 2	99.9%	3.2908	99%	2.326	31.5484	0.025	0.000625	0.338	0.114244	0
Left margin U/Mo zone 3	99.9%	3.2908	99%	2.326	31.5484	0.025	0.000625	0.074	0.005476	4
Left margin U/Mo zone 4	99.9%	3.2908	99%	2.326	31.5484	0.025	0.000625	0.338	0.114244	0
Left margin U/Mo zone 5	99.9%	3.2908	99%	2.326	31.5484	0.025	0.000625	-	-	-
Right margin U/Mo zone 1	99.9%	3.2908	99%	2.326	31.5484	0.025	0.000625	-	-	-
Right margin U/Mo zone 2	99.9%	3.2908	99%	2.326	31.5484	0.025	0.000625	0.338	0.114244	0
Right margin U/Mo zone 3	99.9%	3.2908	99%	2.326	31.5484	0.025	0.000625	0.08	0.006400	3
Right margin U/Mo zone 4	99.9%	3.2908	99%	2.326	31.5484	0.025	0.000625	0.338	0.114244	0
Right margin U/Mo zone 5	99.9%	3.2908	99%	2.326	31.5484	0.025	0.000625	-	-	-
Thickness of U/Mo	99.9%	3.2908	99%	2.326	31.5484	-	-	12 mic	-	-
Mo content	99.9%	3.2908	99%	2.326	31.5484	0.001	0.000001	0.01	0.000100	0
Wt. fraction U-235	99.9%	3.2908	99%	2.326	31.5484	0.001	0.000001	0.001	0.000001	32
Density of U/Mo	99.9%	3.2908	99%	2.326	31.5484	0.001	0.000001	0.17	0.028900	0
Trace elements boron equivalent	99.9%	3.2908	99%	2.326	31.5484	0.001	0.000001	0.01	0.000100	0
Boron loading in plate	99.9%	3.2908	99%	2.326	31.5484	0.05	0.002500	0.1	0.010000	8
Maximum non-bond size (U/Mo to Zr)	99.9%	3.2908	99%	2.326	31.5484	?	?	?	?	?
Maximum non-bond size (Zr to Al)	99.9%	3.2908	99%	2.326	31.5484	?	?	?	?	?
Zircaloy thickness above U/Mo	99.9%	3.2908	99%	2.326	31.5484	2.5	6.250000	5	25.000000	8
Zircaloy thickness below U/Mo	99.9%	3.2908	99%	2.326	31.5484	2.5	6.250000	5	25.000000	8
Zr length beyond U/Mo top	99.9%	3.2908	99%	2.326	31.5484	0.025	0.000625	0.05	0.002500	8
Zr length beyond U/Mo top	99.9%	3.2908	99%	2.326	31.5484	0.025	0.000625	0.05	0.002500	8
Zr Left margin U/Mo zone	99.9%	3.2908	99%	2.326	31.5484	0.025	0.000625	0.05	0.002500	8
Zr Left margin U/Mo zone	99.9%	3.2908	99%	2.326	31.5484	0.025	0.000625	0.05	0.002500	8
Assembled plate thickness	95.0%	1.9604	80%	0.84	7.8422	0.025	0.000625	0.00254	0.000006	760

Table B.7 Sensitivity study using ratios of standard deviation to margin of error

Case A: Standard Deviation < Margin of Error

Case A.1
Standard deviation:Margin of error = 1:1

Confidence	Z_α	Power	Z_β	$(Z_\alpha + Z_\beta)^2$	s	s^2	E	E^2	# of Trials
99.9%	3.2908	99.0%	2.326	31.5484	1	1.00	1	1.00	32
99.9%	3.2908	97.5%	1.96	27.5709	1	1.00	1	1.00	28
99.9%	3.2908	95.0%	1.64	24.3128	1	1.00	1	1.00	24
99.9%	3.2908	90.0%	1.28	20.8922	1	1.00	1	1.00	21
99.9%	3.2908	80.0%	0.84	17.0635	1	1.00	1	1.00	17
99.0%	2.5762	99.0%	2.326	24.0316	1	1.00	1	1.00	24
99.0%	2.5762	97.5%	1.96	20.5771	1	1.00	1	1.00	21
99.0%	2.5762	95.0%	1.64	17.7763	1	1.00	1	1.00	18
99.0%	2.5762	90.0%	1.28	14.8703	1	1.00	1	1.00	15
99.0%	2.5762	80.0%	0.84	11.6704	1	1.00	1	1.00	12
95.0%	1.96	99.0%	2.326	18.3698	1	1.00	1	1.00	18
95.0%	1.96	97.5%	1.96	15.3664	1	1.00	1	1.00	15
95.0%	1.96	95.0%	1.64	12.9600	1	1.00	1	1.00	13
95.0%	1.96	90.0%	1.28	10.4976	1	1.00	1	1.00	10
95.0%	1.96	80.0%	0.84	7.8400	1	1.00	1	1.00	8

Case A.2
Standard deviation:Margin of error = 1:2

Confidence	Z_α	Power	Z_β	$(Z_\alpha + Z_\beta)^2$	s	s^2	E	E^2	# of Trials
99.9%	3.2908	99.0%	2.326	31.5484	1	1.00	2	4.00	8
99.9%	3.2908	97.5%	1.96	27.5709	1	1.00	2	4.00	7
99.9%	3.2908	95.0%	1.64	24.3128	1	1.00	2	4.00	6
99.9%	3.2908	90.0%	1.28	20.8922	1	1.00	2	4.00	5
99.9%	3.2908	80.0%	0.84	17.0635	1	1.00	2	4.00	4
99.0%	2.5762	99.0%	2.326	24.0316	1	1.00	2	4.00	6
99.0%	2.5762	97.5%	1.96	20.5771	1	1.00	2	4.00	5
99.0%	2.5762	95.0%	1.64	17.7763	1	1.00	2	4.00	4
99.0%	2.5762	90.0%	1.28	14.8703	1	1.00	2	4.00	4
99.0%	2.5762	80.0%	0.84	11.6704	1	1.00	2	4.00	3
95.0%	1.96	99.0%	2.326	18.3698	1	1.00	2	4.00	5
95.0%	1.96	97.5%	1.96	15.3664	1	1.00	2	4.00	4
95.0%	1.96	95.0%	1.64	12.9600	1	1.00	2	4.00	3
95.0%	1.96	90.0%	1.28	10.4976	1	1.00	2	4.00	3
95.0%	1.96	80.0%	0.84	7.8400	1	1.00	2	4.00	2

Table 7 (continued)

Case A.3
Standard deviation:Margin of error = 1:3

Confidence	Z_α	Power	Z_β	$(Z_\alpha + Z_\beta)^2$	s	s^2	E	E^2	# of Trials
99.9%	3.2908	99.0%	2.326	31.5484	1	1.00	3	9.00	4
99.9%	3.2908	97.5%	1.96	27.5709	1	1.00	3	9.00	3
99.9%	3.2908	95.0%	1.64	24.3128	1	1.00	3	9.00	3
99.9%	3.2908	90.0%	1.28	20.8922	1	1.00	3	9.00	2
99.9%	3.2908	80.0%	0.84	17.0635	1	1.00	3	9.00	2
99.0%	2.5762	99.0%	2.326	24.0316	1	1.00	3	9.00	3
99.0%	2.5762	97.5%	1.96	20.5771	1	1.00	3	9.00	2
99.0%	2.5762	95.0%	1.64	17.7763	1	1.00	3	9.00	2
99.0%	2.5762	90.0%	1.28	14.8703	1	1.00	3	9.00	2
99.0%	2.5762	80.0%	0.84	11.6704	1	1.00	3	9.00	1
95.0%	1.96	99.0%	2.326	18.3698	1	1.00	3	9.00	2
95.0%	1.96	97.5%	1.96	15.3664	1	1.00	3	9.00	2
95.0%	1.96	95.0%	1.64	12.9600	1	1.00	3	9.00	1
95.0%	1.96	90.0%	1.28	10.4976	1	1.00	3	9.00	1
95.0%	1.96	80.0%	0.84	7.8400	1	1.00	3	9.00	1

Case A.4
Standard deviation:Margin of error = 1:4

Confidence	Z_α	Power	Z_β	$(Z_\alpha + Z_\beta)^2$	s	s^2	E	E^2	# of Trials
99.9%	3.2908	99.0%	2.326	31.5484	1	1.00	4	16.00	2
99.9%	3.2908	97.5%	1.96	27.5709	1	1.00	4	16.00	2
99.9%	3.2908	95.0%	1.64	24.3128	1	1.00	4	16.00	2
99.9%	3.2908	90.0%	1.28	20.8922	1	1.00	4	16.00	1
99.9%	3.2908	80.0%	0.84	17.0635	1	1.00	4	16.00	1
99.0%	2.5762	99.0%	2.326	24.0316	1	1.00	4	16.00	2
99.0%	2.5762	97.5%	1.96	20.5771	1	1.00	4	16.00	1
99.0%	2.5762	95.0%	1.64	17.7763	1	1.00	4	16.00	1
99.0%	2.5762	90.0%	1.28	14.8703	1	1.00	4	16.00	1
99.0%	2.5762	80.0%	0.84	11.6704	1	1.00	4	16.00	1
95.0%	1.96	99.0%	2.326	18.3698	1	1.00	4	16.00	1
95.0%	1.96	97.5%	1.96	15.3664	1	1.00	4	16.00	1
95.0%	1.96	95.0%	1.64	12.9600	1	1.00	4	16.00	1
95.0%	1.96	90.0%	1.28	10.4976	1	1.00	4	16.00	1
95.0%	1.96	80.0%	0.84	7.8400	1	1.00	4	16.00	0

Case A.5
Standard deviation:Margin of error = 1:5

Confidence	Z_α	Power	Z_β	$(Z_\alpha + Z_\beta)^2$	s	s^2	E	E^2	# of Trials
99.9%	3.2908	99.0%	2.326	31.5484	1	1.00	5	25.00	1
99.9%	3.2908	97.5%	1.96	27.5709	1	1.00	5	25.00	1
99.9%	3.2908	95.0%	1.64	24.3128	1	1.00	5	25.00	1
99.9%	3.2908	90.0%	1.28	20.8922	1	1.00	5	25.00	1
99.9%	3.2908	80.0%	0.84	17.0635	1	1.00	5	25.00	1
99.0%	2.5762	99.0%	2.326	24.0316	1	1.00	5	25.00	1
99.0%	2.5762	97.5%	1.96	20.5771	1	1.00	5	25.00	1
99.0%	2.5762	95.0%	1.64	17.7763	1	1.00	5	25.00	1
99.0%	2.5762	90.0%	1.28	14.8703	1	1.00	5	25.00	1
99.0%	2.5762	80.0%	0.84	11.6704	1	1.00	5	25.00	0
95.0%	1.96	99.0%	2.326	18.3698	1	1.00	5	25.00	1
95.0%	1.96	97.5%	1.96	15.3664	1	1.00	5	25.00	1
95.0%	1.96	95.0%	1.64	12.9600	1	1.00	5	25.00	1
95.0%	1.96	90.0%	1.28	10.4976	1	1.00	5	25.00	0
95.0%	1.96	80.0%	0.84	7.8400	1	1.00	5	25.00	0

Case B:
Standard Deviation < Margin of Error

Case B.1
Standard deviation: Margin of error = 2:1

Confidence	Z_α	Power	Z_β	$(Z_\alpha + Z_\beta)^2$	s	s^2	E	E^2	# of Trials
99.9%	3.2908	99.0%	2.326	31.5484	2	4.00	1	1.00	126
99.9%	3.2908	97.5%	1.96	27.5709	2	4.00	1	1.00	110
99.9%	3.2908	95.0%	1.64	24.3128	2	4.00	1	1.00	97
99.9%	3.2908	90.0%	1.28	20.8922	2	4.00	1	1.00	84
99.9%	3.2908	80.0%	0.84	17.0635	2	4.00	1	1.00	68
99.0%	2.5762	99.0%	2.326	24.0316	2	4.00	1	1.00	96
99.0%	2.5762	97.5%	1.96	20.5771	2	4.00	1	1.00	82
99.0%	2.5762	95.0%	1.64	17.7763	2	4.00	1	1.00	71
99.0%	2.5762	90.0%	1.28	14.8703	2	4.00	1	1.00	59
99.0%	2.5762	80.0%	0.84	11.6704	2	4.00	1	1.00	47
95.0%	1.96	99.0%	2.326	18.3698	2	4.00	1	1.00	73
95.0%	1.96	97.5%	1.96	15.3664	2	4.00	1	1.00	61
95.0%	1.96	95.0%	1.64	12.9600	2	4.00	1	1.00	52
95.0%	1.96	90.0%	1.28	10.4976	2	4.00	1	1.00	42
95.0%	1.96	80.0%	0.84	7.8400	2	4.00	1	1.00	31

Case B.2
Standard deviation: Margin of error = 3:1

Confidence	Z_α	Power	Z_β	$(Z_\alpha + Z_\beta)^2$	s	s^2	E	E^2	# of Trials
99.9%	3.2908	99.0%	2.326	31.5484	3	9.00	1	1.00	284
99.9%	3.2908	97.5%	1.96	27.5709	3	9.00	1	1.00	248
99.9%	3.2908	95.0%	1.64	24.3128	3	9.00	1	1.00	219
99.9%	3.2908	90.0%	1.28	20.8922	3	9.00	1	1.00	188
99.9%	3.2908	80.0%	0.84	17.0635	3	9.00	1	1.00	154
99.0%	2.5762	99.0%	2.326	24.0316	3	9.00	1	1.00	216
99.0%	2.5762	97.5%	1.96	20.5771	3	9.00	1	1.00	185
99.0%	2.5762	95.0%	1.64	17.7763	3	9.00	1	1.00	160
99.0%	2.5762	90.0%	1.28	14.8703	3	9.00	1	1.00	134
99.0%	2.5762	80.0%	0.84	11.6704	3	9.00	1	1.00	105
95.0%	1.96	99.0%	2.326	18.3698	3	9.00	1	1.00	165
95.0%	1.96	97.5%	1.96	15.3664	3	9.00	1	1.00	138
95.0%	1.96	95.0%	1.64	12.9600	3	9.00	1	1.00	117
95.0%	1.96	90.0%	1.28	10.4976	3	9.00	1	1.00	94
95.0%	1.96	80.0%	0.84	7.8400	3	9.00	1	1.00	71

Case B.3
Standard deviation:Margin of error = 4:1

Confidence	Z_α	Power	Z_β	$(Z_\alpha + Z_\beta)^2$	s	s^2	E	E^2	# of Trials
99.9%	3.2908	99.0%	2.326	31.5484	4	16.00	1	1.00	505
99.9%	3.2908	97.5%	1.96	27.5709	4	16.00	1	1.00	441
99.9%	3.2908	95.0%	1.64	24.3128	4	16.00	1	1.00	389
99.9%	3.2908	90.0%	1.28	20.8922	4	16.00	1	1.00	334
99.9%	3.2908	80.0%	0.84	17.0635	4	16.00	1	1.00	273
99.0%	2.5762	99.0%	2.326	24.0316	4	16.00	1	1.00	385
99.0%	2.5762	97.5%	1.96	20.5771	4	16.00	1	1.00	329
99.0%	2.5762	95.0%	1.64	17.7763	4	16.00	1	1.00	284
99.0%	2.5762	90.0%	1.28	14.8703	4	16.00	1	1.00	238
99.0%	2.5762	80.0%	0.84	11.6704	4	16.00	1	1.00	187
95.0%	1.96	99.0%	2.326	18.3698	4	16.00	1	1.00	294
95.0%	1.96	97.5%	1.96	15.3664	4	16.00	1	1.00	246
95.0%	1.96	95.0%	1.64	12.9600	4	16.00	1	1.00	207
95.0%	1.96	90.0%	1.28	10.4976	4	16.00	1	1.00	168
95.0%	1.96	80.0%	0.84	7.8400	4	16.00	1	1.00	125

Case B.4
Standard deviation:Margin of error = 5:1

Confidence	Z_α	Power	Z_β	$(Z_\alpha + Z_\beta)^2$	s	s^2	E	E^2	# of Trials
99.9%	3.2908	99.0%	2.326	31.5484	5	25.00	1	1.00	789
99.9%	3.2908	97.5%	1.96	27.5709	5	25.00	1	1.00	689
99.9%	3.2908	95.0%	1.64	24.3128	5	25.00	1	1.00	608
99.9%	3.2908	90.0%	1.28	20.8922	5	25.00	1	1.00	522
99.9%	3.2908	80.0%	0.84	17.0635	5	25.00	1	1.00	427
99.0%	2.5762	99.0%	2.326	24.0316	5	25.00	1	1.00	601
99.0%	2.5762	97.5%	1.96	20.5771	5	25.00	1	1.00	514
99.0%	2.5762	95.0%	1.64	17.7763	5	25.00	1	1.00	444
99.0%	2.5762	90.0%	1.28	14.8703	5	25.00	1	1.00	372
99.0%	2.5762	80.0%	0.84	11.6704	5	25.00	1	1.00	292
95.0%	1.96	99.0%	2.326	18.3698	5	25.00	1	1.00	459
95.0%	1.96	97.5%	1.96	15.3664	5	25.00	1	1.00	384
95.0%	1.96	95.0%	1.64	12.9600	5	25.00	1	1.00	324
95.0%	1.96	90.0%	1.28	10.4976	5	25.00	1	1.00	262
95.0%	1.96	80.0%	0.84	7.8400	5	25.00	1	1.00	196

As we test the plates and compare the number of plates to our expected number of failures, nominally 1 in every 540, how can we be certain that we have tested all of the existing parameters? In other words, how do we know that there are not any unknown variables that haven't been tested or controlled and could cause the fuel plates to fail if their values vary beyond the acceptable margin of error (the unknown unknowns)? By testing the plates, if we produce more failures than we had previously expected, we can deduce that there is at least one "unknown parameter." Further tests can be conducted and plates can be inspected to qualify the parameter. Otherwise, if our plate tests conclude that our failure rates are within the acceptable range, we can report with our given level of confidence that our fuel specification has included all needed tests, and that our fuel plates meet the requirements for LEU fuel and will operate successfully inside HFIR.

The analyses presented here are based on the assumption that our measurements are independent of each other. This is not strictly true but the assumption is conservative in that it will result in a greater number of plates being required for testing at a given confidence level than would be found necessary if co-variances were considered.

B.1 References

B.1. Cochran: Sampling Techniques Introduction, Apr. 2007, 22 June 2009,<http://www.gap-system.org/~history/Extras/Cochran_sampling_intro.html>.

B.2. Bartlette, II, James E., Joe W. Kotrlik, and Chadwick C. Higgins, "Organizational Research: Determining Appropriate Sample Size in Survey Research," Information Technology, Learning, and Performance Journal 19 (2001): 43-50, Organizational Systems Research Association, 22 June 2009 <http://www.osra.org/itlpj/ bartlettkotrlikhiggins.pdf>.

B.3. Bluman, Alan G., ed. Elementary Statistics: A Step by Step Approach: A Brief Version, 4th ed. Addison-Wesley, 1999.

B.4. Determining Sample Size, 2009, University of Florida, 22 June 2009 <http://edis.ifas.ufl.edu/PD006>.

B.5. Measuring Usability. 2004. Measuring Usability LLC. 1 July 2009 <http://www.measuringusability.com/zcalcp.php#relatedqs>.

APPENDIX C

EXAMPLES OF SIMILAR STATISTICAL STUDIES

In order to familiarize the reader with formula B.1 in Appendix B, the following examples from real-world statistical problems are provided.

Example 1:
A cardiologist studying a particular genetic mutation that causes HCM (Hypertrophic cardiomyopathy, a common congenital heart disorder) wishes to estimate the mean left ventricular mass of patients with this particular mutation within 10g and compare it to the mean for other patients with HCM. If previous laboratory measurements suggest a standard deviation of 30g and he chooses a significance 95% confidence level, and a power of 90%, what size sample does he need?

$$N = \frac{(1.960 + 1.282)^2 * (30)^2}{10^2} = 94.6 = 95$$

Adapted from Ref. C.1.

Example 2:
We are doing an experiment to test topical anesthetics. The sample size calculation consisted of an α level (type I error) rate of 0.01 for a two-tailed test and a β level (type II error) rate of 0.05. In both cases, we selected values at a more rigorous level than the standard α level of 0.05 and β level of 0.20. For the calculation, we used the standard deviations from topical anesthetic studies that also measured pain on injection using a VAS, which equaled 20. We estimated that a difference of 20 mm on a 100-mm VAS would be considered clinically significant when comparing one group with another (precision/margin of error). The formula for the sample size calculation is

$$N = \frac{(2.58 + 1.64)^2 * (20)^2}{20^2} = 17.8 = 18$$

Adapted from Ref. C.2.

Example 3
Suppose that a chemical that reduces appetite is to be tested to learn whether it alters the body weight of rats. In previous experiments, the mean body weight of the rats used was 400g, with a standard deviation of 23g. Assume also that the scientist would like to be able to detect the change with a power (1-β) of 90% and 95% confidence. The use of the chemical causes of weight loss of 30g, with a standard deviation of 20 g and a margin of error of 10 g. How many mice should be used in the experiment?

$$N = \frac{(1.96 + 1.28)^2 * (20)^2}{10^2} = 41.99 = 42$$

Adapted from Ref. C.3.

Example 4:
A fast food company wants to determine the average number of times that fast food users visit fast food restaurants per week. They have decided that their estimate needs to be accurate within plus or minus one-tenth of a visit, and they want to be 95% sure that their estimate does not differ from true number of visits by more than one-tenth of a visit, with a power of 80%. Previous research has shown that the standard deviation is .7 visits. What is the required sample size?

$$N = \frac{(1.96 + 0.84)^2 * (0.7)^2}{0.1^2} = 384.16 = 385$$

Adapted from Ref. C.4.

C.1 References

C.1. Gallin, John I., and Frederick P. Ognibene, eds., Principles and Practice of Clinical Research. New York: Academic P, 2002.

C.2. Jacobs, Shawn, Daniel A. Haas, John G. Meechan, and Sherry May, "Injection pain: Comparison of three mandibular block techniques and modulation by nitrous oxide:oxygen," The Journal of the American Dental Association, 2009, 7 July 2009 http://jada.ada.org/cgi/reprint/134/7/869.pdf?referer=www.clickfind.com.au.

C.3. Committee, and Guidelines for the Care and Use of Mammals in Neuroscience and Behavioral Research, National Research Council, New York: National Academies P, 2003.

C.4. The Statistics Calculator: Statistical Analysis Tests At Your Fingertips. 2009. StatPac Inc. 14 July 2009 <http://www.statpac.com/statistics-calculator/sampling.htm>.

INTERNAL DISTRIBUTION

1. K. J. Beierschmitt (*beierschmitt@ornl.gov*)
2. C. A. Blue (*blueca@ornl.gov*)
3. S. E. Burnette (*burnettese@ornl.gov*)
4. D. C. Christensen (*christensend@ornl.gov*)
5. D. H. Cook *(dhc@ornl.gov)*
6. B. S. Cowell (*cowellbs@ornl.gov*)
7. R. A. Crone (*cronera@ornl.gov*)
8. R. J. Ellis (*ellisrj@ornl.gov*)
9. J. D. Freels *(freelsjd@ornl.gov)*
10. J. C. Gehin (*gehinjc@ornl.gov*)
11. G. Ilas (*ilasg@ornl.gov*)
12. B. C. Jolly (jollybc@ornl.gov)
13. J. H. Miller (*millerjh2@ornl.gov*)
14. L. J. Ott (*ottlj@ornl.gov*)
15. C. V. Parks (*parkscv@ornl.gov)*

16–18. R. T. Primm III (*primmrtiii@ornl.gov*)

19. R. R. Rawl (*rawlrr@ornl.gov*)
20. D. G. Renfro (*renfrodg@ornl.gov)*
21. A. W. Riedy (*riedyaw@ornl.gov*)
22. J. E. Rushton (*rushtonje@ornl.gov*)
23. L. J. Satkowiak (*satkowiaklj@ornl.gov*)
24. J. D. Sease (*seasejd@ornl.gov*)
25. K. A. Smith (*smithka@ornl.gov*)
26. R. L. Snipes (*snipesrl@ornl.gov*)
27. S. J. Zinkle (*zinklesj@ornl.gov*)
28. ORNL Laboratory Records (*hamrindr@ornl.gov*)

EXTERNAL DISTRIBUTION

29. A. Adams, U.S. Nuclear Regulatory Commission, One White Flint North, 11555 Rockville Pike, Rockville, Maryland 20852-2738 (*axa@nrc.gov*)
30. T. Andes, BWXT/Y-12, Y-12 National Security Complex, P.O. Box 2009, Oak Ridge, TN 37831-8245 (*andestc@y12.doe.gov*)
31. R. A. Butler, Director, Research Reactor Center, 1513 Research Park Drive, Columbia, MO 65211 (*ButlerRa@missouri.edu*)
32. G. S. Chang, Idaho National Laboratory, P.O. Box 1625, Idaho Falls, ID 83415-3885 (*gray.chang@inl.gov*)
33. D. Chong, NA-212, U.S. Department of Energy, 1000 Independence Avenue SW, Washington, DC 20585 (*Daniel.Chong@nnse.doe.gov*)
34. H. E. Clark, U.S. Department of Energy Oak Ridge Office, P.O. Box 2001, Oak Ridge, TN 37831 (*hkc@ornl.gov*)
35. D. Diamond, Brookhaven National Laboratory, P.O. Box 5000, Upton, NY 11973-5000 (*diamond@bnl.gov*)
36. Roger Klaffky, Office of Basic Energy Sciences, U.S. Department of Energy, 1000 Independence Avenue SW, Washington, DC 20585 (*roger.klaffky@science.doe.gov).*
37. H. D. Gougar, Manager, Fission & Fusion Systems, INEEL, P.O. Box 1625, MS 3860, Idaho Falls, ID 83415-3860 (*goughd@inl.gov*)
38. Sean O'Kelly, NIST Center for Neutron Research, 100 Bureau Drive, Stop 8560, Gaithersburg, MD 20899-8560 (*sean.okelly@nist.gov*)
39. Kathy Garcia, NA-212, U.S. Department of Energy, 1000 Independence Avenue SW, Washington, DC 20585 (*Kathy.Garcia@nnsa.doe.gov*)
40. D. Kutikkad, Assistant Reactor Manager-Physics, University of Missouri Research Reactor Facility, Columbia, MO 65211 (*kutikkadk@missouri.edu*)
41. J. Matos, Argonne National Laboratory, 9700 S. Cass Avenue, Argonne, IL 60439 (*jim.matos@anl.gov*)
42. C. McKibben, University of Missouri Research Reactor Facility, Columbia, MO 65211 (*mckibben@missouri.edu*)
43. D. M. Hewitt, Idaho National Laboratory, P.O. Box 1625, Idaho Falls, ID 83415-3750 (*Dana.Hewitt@inl.gov*)
44. T. Newton, MIT Nuclear Reactor Laboratory, 138 Albany St., Cambridge, MA 02139 (*tnewton@mit.edu*)
45. W. Richards, NIST Center for Neutron Research, 100 Bureau Drive, Stop 8561, Gaithersburg, MD 20899-8561 (*wade.richards@nist.gov*)
46. W. C. Richardson, BWXT Technology, Inc., 2016 Mount Athos Rd., Lynchburg, VA 24504 (*WCRichardson@bwxt.com*)

47. J. Roglans, Argonne National Laboratory, 9700 S. Cass Avenue, Argonne, IL 60439 (*roglans@anl.gov*)
48. J. Snelgrove, Argonne National Laboratory, 9700 S. Cass Avenue, Argonne, IL 60439 (*jimsnelgrove@anl.gov*)
49. P. Staples, NA-212, U.S. Department of Energy, 1000 Independence Avenue SW, Washington, DC 20585 (*Parrish.Staples@nnsa.doe.gov*)
50. Daniel M. Wachs, MFC 791 B-147, Idaho National Laboratory, P.O. Box 6188, Idaho Falls, ID 83415 (*Daniel.Wachs@inl.gov*)
51. R. E. Williams, NIST Center for Neutron Research, 100 Bureau Drive, Stop 8560, Gaithersburg, MD 20899-8560 (*robert.williams@nist.gov*)
52. John Stevens, Argonne National Laboratory, 9700 S. Cass Avenue, Argonne, IL 60439 (*johnstevens@anl.gov*)
53. Tracey Guida, University of Pittsburgh, Pittsburgh, PA, 15260 (*tlg29+@pitt.edu*)
54. Eric C Woolstenhulme, P.O. Box 1625, Idaho Falls, ID 83415-3750 (*Eric.Woolstenhulme@inl.gov*)
55. Pedro Mantano, Office of Basic Energy Sciences, U.S. Department of Energy, 1000 Independence Avenue SW, Washington, DC 20585 (*pedro.montano@science.doe.gov).*
56. Carol Sohn, of Basic Energy Sciences, U.S. Department of Energy (*carol.sohn@pnso.science.doe.gov).*
57. Johnny O. Moore, U. S. Department of Energy, (*moorejo@ornl.gov*)